Article

Not peer-reviewed version

Geological and Geochemical Characterization of Variscan Pegmatites in the Sidi Bou Othmane District, Central Jebilet Province, Morocco: Insights about Their Potential as a Source of Raw Materials

Amina Wafik , Nouamane El Aouad , Youssef Daafi , Yousra Morsli , Marouane Chniouar , Rosalda Punturo , Aida Maria Conte , Daniela Guglietta * , Wissale Aba Sidi

Posted Date: 25 December 2023

doi: 10.20944/preprints202312.1793.v1

Keywords: Central Jebilet; Sidi Bou Othmane; Pegmatite dykes; syn-collision; S-granite

Article

Geological and Geochemical Characterization of Variscan Pegmatites in the Sidi Bou Othmane District, Central Jebilet Province, Morocco: Insights about Their Potential as a Source of Raw Materials

Amina Wafik [1], Nouamane El Aouad [1,2], Youssef Daafi [3], Yousra Morsli [4], Marouane Chniouar [1], Rosalda Punturo [5,6], Aida Maria Conte [6], Daniela Guglietta [6,*] and Wissale Aba Sidi [1,2]

[1] DLGR Laboratory, Faculty of Sciences Semlalia, Cadi Ayyad University, Marrakech 40000, Morocco; wafik@uca.ac.ma (A.W.); nouaman.geomine@gmail.com (N.E.A.); Marouane Chniouar marouanechniouar@gmail.com (M.C.);
[2] Applied Geophysics, Water and Environment Laboratory, Faculty of Sciences and Technics, Molay Slimane University, Béni Mellal, Morocco abasidiwissale1@gmail.com (W.A.S.)
[3] OCP Group, bd Moulay Youssef, 46300, Youssoufia, Morocco DAAFI@ocpgroup.ma (Y.D.)
[4] Geosciences and Applications Laboratory, Faculty of Sciences Ben Msik, Casablanca, Morocco yousramorsli@gmail.com (Y.M.)
[5] Department of Biological, Geological and Environmental Sciences, University of Catania, Italy rosalda.punturo@unict.it (R.P.)
[6] Institute of Environmental Geology and Geoengineering, National Research Council of Italy (CNR IGAG), Research Area of Rome 1, 00010 Rome, Italy; aidamaria.conte@cnr.it (A.M.C.)
* Correspondence: daniela.guglietta@cnr.it (D.G.).

Abstract: The Sidi Bou Othmane (SBO) pegmatite district is in the Central Jebilet massif, Occidental Meseta domain, Morocco. The SBO district is hosted essentially in a volcano-sedimentary series composed of the Late-Devonian Sarhlef shales. Pegmatite bodies crop out as dykes, which are oriented from N-S to E-W and are generally variably deformed with ductile and/or brittle structures with ante, syn- or post kinematic criteria. Petrographic observations of pegmatite dykes show that feldspars (i.e., albite, microcline) are the most abundant mineral phases, followed by quartz, micas, with tourmaline and accessory mineral as garnet, and zircon and secondary minerals as clinochlore, sericite, and illite. The geochemical study indicates that, according to the major pegmatite elements dykes of SBO have mainly a S-type granitic composition and are peraluminous granite with calc-alkalic affinity. The study of trace elements pointed out that SBO pegmatite formed under post-orogenic syn-collision context during the Variscan orogeny, by the partial melting of argilliferous sediment and can be ascribed to the muscovite-bearing pegmatite; moreover, they have a good potential on ceramic and contain minerals, such as feldspar, recently assessed as Critical raw materials by European Union.

Keywords: central Jebilet; Sidi Bou Othmane; pegmatite dykes; syn-collision; S-granite

1. Introduction

Pegmatite has been specified as an igneous rock of mostly granitic composition, with properties such as highly coarsened and generally variable crystals, an abundance of strongly directional graphitic or other skeletal crystal growth, and the prominent spatial zonation of mineral assemblages, including monomineralic zones [1,2,3,4].

Granitic pegmatites are the main host rocks for rare metal deposits, strategic minerals, and precious/ semi-precious gems [5]. They are commonly interpreted as the end products of extreme fractional crystallization of granitic magmas. This fractionation promotes the increase of rare metals

 doi:10.20944/preprints202312.1793.v1

and volatiles in the residual melt, leading to the development of mineralization in granitic pegmatites [6,7].

In Morocco, granitic pegmatites hosted in Precambrian terrains are relatively the most studied [8,9,10,11,12,13,14,15,16,17]. The few works conducted on Variscan pegmatites and more precisely on those ones of the Jebilet Massif dates to some decades ago [18,19,20,21,22,23] and mainly deal with the crystallography of the phosphatic mineral phases occurring within these pegmatite rocks; moreover, these works have shown the presence of frequent monocrystalline ferrisicklerite nodules in the veins of SBO pegmatite (Jebilet Massif).

Recently, Essaifi et al., [24] pointed out that, the shear zones affecting the Tabouchent granodiorite allowed fluid flow at a regional scale, causing the metal zonation observed around the pluton from a proximal Cu-Au mineralization to Ag-Pb-Zn-Au mineralization.

The Jebilet Massif represents a critical mining district, characterized by various ore deposits (e.g., Draa Sfar VMS, Frag al Ma graphite field graphite, SBO -Sidi Bou Othmane- district aplo-pegmatite). It is noteworthy that the SBO pegmatites and Bir Nhass reflect a good example because they have never been the subject of an intense geological study or a well-detailed mapping. Indeed, despite geological research carried out on the Jebilet Massif during the last decades [25,26,27], only a few data are available on SBO pegmatites. Precise petrological and geochemical data and spatial distribution and relationships with surrounding rocks and the deformation are still unclear.

This study aims to characterize the, petrographic and geochemical featutes of the SBO pegmatites, identify their associated alteration, and classify them.

2. Geological setting

The study area is located at about thirty kilometers in the North of Marrakesh (Morocco). It is geologically situated in the central unit of Jebilet in the Mestian domain (**Figure 1**) [26, 28,29,30]. A folded Hercynian chain characterizes formed essentially by a Paleozoic basement, metamorphosed into greenschist to amphibolite facies, and intruded by syn- to late orogenic magmatic intrusions during the Variscan orogeny [31,32], outcropping in an undeformed Mesozoic to Cenozoic cover.

Preprints (www.preprints.org) | NOT PEER-REVIEWED | Posted: 25 December 2023 doi:10.20944/preprints202312.1793.v1

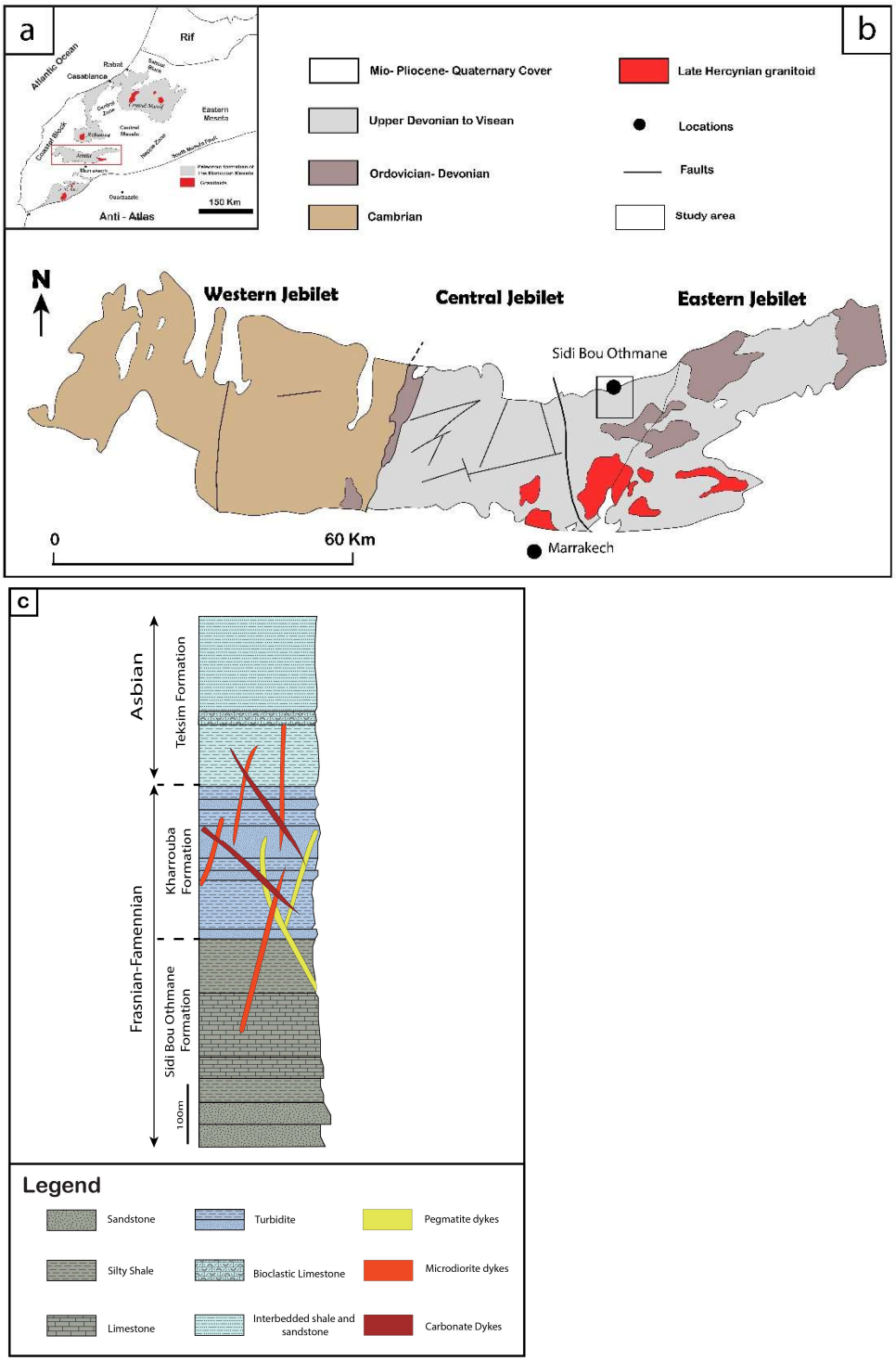

Figure 1. (**a**) Localization of the Jebilet massif in the Variscan of Morocco; (b) Geological Context of the Variscan Jebilet Massifs showing the location of Sidi Bou Othmane study area modified from, Huvelin [28], (**c**) Synthetic lithostratigraphic column of the Sidi Bou Othmane area in the Jebilet Massif modified after Bordonaro [30], Delchini [28], Lazreq et al., [29].

The SBO area presents three main geological formations [29,33]:

- a lower formation named Sidi Bou Othmane formation, mainly constituted of sandstones, silty shale, and limestone;
- a middle formation named Kharrouba formation, formed essentially by turbidites, these two series are cut by numerous dykes (pegmatites, microdiorite, carbonates) and formed during Frasnian-Famennian;

 doi:10.20944/preprints202312.1793.v1

- an upper formation (Asbian) called Teksim formation, which corresponds to a transgressive series deposited in a platform environment composed of shales, limestones, sandstones, and siltstones.

Numerous acid and basic magmatic bodies characterize the central part of the Jebilet Massif. The emplacement of these magma bodies is related to Hercynian deformation and is subdivided into three episodes: the pre-tectonic; the orogenic; and the post-orogenic episode [28]. Mrini et al., [34], dated these magmatic bodies by using the Rb–Sr method on whole rocks, and gave ages of 330 and 250 Ma, respectively. The orogenic granites of mixed origin and leucogranites of crustal origin were emplaced between 330 Ma and 280-275 Ma and show calc-alkaline affinities. The late orogenic granite and leucogranites of crustal origin are younger and intruded the granodiorite, date between 275 Ma and 250 Ma. They are mainly alkaline. It is worth noting that recent dating, suggests older ages up to 358 Ma [26].

The Carboniferous fields underwent a very intense deformation showing that the Hercynian orogeny stretched out between 330 and 250 Ma [34]. This deformation is the result of a succession of tectonic events contemporary to the Hercynian and post-Hercynian orogeny. Bordonaro [30], summarized five stages of deformation in central Jebilet (D0, D1, D2, D3, D4):

- D0 ante-schist deformation with large-scale E-W folds, related to the syn-sedimentary strike-slip sheets of the Eastern Jebilet;
- D1 deformation is marked by a syn-schistosity folding of average direction N30 with a slightly sloping axial plane in the East and rectified in the West; this is a regional syn-metamorphism;
- D2 deformation coincides with the paroxysm of the deformation and metamorphism; it is characterized by folding and shearing the D1 structures;
- D3 deformation is characterized by a N110 to N150 crenulation schistosity sloping towards the NE and very localized thrusting towards the West;
- D4 deformation is represented by two sets of conjugate N70 dextral and N135 sinistral strike-slip faults. Zig-zag folds are also observable.

These areas underwent a sub meridian syn-schist folding phase, associated with epizonal metamorphism of post-upper Visean age, followed by sub-parallel shearing at S1 [35]. However, there is also the existence of a peri-plutonic metamorphism that developed around granite intrusions; the brittle tectonics is marked mainly by the existence of directional faults generally from N70° to N90°, sinistral strike-slip fault [36].

3. Materials and Methods

The fieldwork provided a detailed geological mapping of the pegmatite dykes, structural measurements, and a large sampling within these dykes and their host rocks. Slides of fresh samples of pegmatite carefully selected from field collections were then prepared and used for minero-petrographic-and geochemical investigation. Minero-petrographic observations have been carried out with a Zeiss Axiolab polarizing microscope on thin sections. About forty thin sections were prepared and observed at the Dynamic of the Lithosphere and Resources Genesis Laboratory (Faculty of Sciences of Semlalia, UCA, Marrakesh). The sample data base, showing the observed minerals and grain size is set out on Table 1.

On the basis of petrographic observations, twenty-five representative samples were then analyzed for major, trace, and rare earth elements, at Laboratories Reminex (Managem Group) using inductively-coupled plasma atomic emission spectrophotometry (ICP-AES),.the major elements are determined using a WD-XRF spectrometer equipped with five diffraction crystals, using fusion glasses made from a mixture of powdered sample and lithium tetraborate ($Li_2B_4O_7$) in the ratio of 1.5. Calibration was based on 30 certified international standards. The trace and rare earth elements are analyzed by ICP-MS. Laser ablation parameters were as follows: spot diameter = 90 μm, frequency = 10 Hz, energy density 20 J/cm2 in a helium ablation medium. The NIST glass reference material SRM 610 was used as the calibration standard. The analytical accuracy for ICP-MS analyses ranged from ± 2–12% with an accuracy of ± 1–8%.

 doi:10.20944/preprints202312.1793.v1

Table 1. Sampling data base reporting, for each selected rock specimen, the mineralogical content, the average grain size, and the host rock.

Sample references	Mineralogical content (accessory minerals to be added as well!)	Grain Size	Host rock
SBO.01	Quartz, Muscovite, Feldspar (apatite, zircon)	<3.5cm	Shale
SBO.02	Quartz, Muscovite, Feldspar (apatite, zircon)	<1.5cm	Shale
SBO.03	Quartz, Muscovite, Feldspar(apatite, zircon)	<1cm	Shale
SBO.04	Quartz, Feldspar, Tourmaline, Muscovite (apatite, zircon)	1-3cm	Shale
SBO.05	Quartz, Feldspar, Muscovite (apatite, zircon)	0.5cm-3.5cm	Shale
SBO.06	Quartz, Feldspar, Muscovite (apatite, zircon)	1-3cm	Shale
SBO.07	Quartz, Feldspar, Muscovite (apatite, zircon)	<0.5cm	Shale
SBO.08	Quartz, Feldspar, Tourmaline, Muscovite (apatite, zircon)	<4.5cm	Shale
SBO.09	Quartz, Feldspar, Muscovite, Tourmaline (apatite, zircon)	<1.5cm	Shale
SBO.10	Quartz, Muscovite, Feldspar (apatite, zircon)	<2.5cm	Shale
SBO.11	Quartz, Muscovite, Feldspar (apatite, zircon)	0.5-1.5cm	Shale
SBO.12	Quartz, Feldspar, Muscovite (apatite, zircon)	<3cm	Shale
SBO.13	Muscovite, Feldspar, Quartz (apatite, zircon)	<1.5cm	Shale
SBO.14	Quartz, Feldspar, Muscovite, Tourmaline (apatite, zircon)	0.5-3.5cm	Shale
SBO.15	Quartz, Muscovite, Feldspar, Tourmaline (apatite, zircon)	1-5cm	Shale
SBO.16	Quartz, Feldspar, Muscovite, Tourmaline (apatite, zircon)	2-4.5cm	Shale
SBO.17	Quartz, Muscovite, Feldspar, Tourmaline (apatite, zircon)	2-10cm	Shale
SBO.18	Quartz, Feldspar, Muscovite (apatite, zircon)	1-4.5cm	Shale
SBO.19	Quartz, Muscovite (apatite, zircon)	<2.5cm	Shale
SBO.20	Quartz, Feldspar, Muscovite (apatite, zircon)	<3cm	Shale
SBO.21	Quartz, Feldspar, Muscovite (apatite, zircon)	<2.5	Shale
SBO.22	Quartz, Feldspar, Muscovite (apatite, zircon)	<3cm	Shale
SBO.23	Quartz, Muscovite, Feldspar (apatite, zircon)	<1.5cm	Shale
SBO.24	Quartz, Feldspar, Muscovite (apatite, zircon)	<0.3cm	Shale
SBO.25	Feldspar, Muscovite, Quartz (apatite, zircon)	<0.9cm	Shale

4. Results

This section, divided by subheadings provides a description of the study pegmatite outcrops and analytical results, their interpretation, as well as the experimental conclusions that can be drawn.

4.1. Pegmatites description

Preprints (www.preprints.org) | NOT PEER-REVIEWED | Posted: 25 December 2023 doi:10.20944/preprints202312.1793.v1

The SBO region is characterized by the abundance of pegmatite rocks forming veins and dykes around the area. The occurrence of pegmatite rocks suggests a shallow magma body [28,37,38]. Other magmatic products are present in the SBO region, they are represented by microdiorite dikes posterior to the pegmatite veins and to the regional schistosity. Their emplacement is related to rifting during the opening of the Atlantic Ocean [28].

The pegmatites of SBO crop out as dykes mainly oriented N30° (N-S to NNE-SSW) with subvertical dip (Figure 2). The field investigations show that E-W dykes are secant on NS pegmatite dykes. Their thickness varies from a few centimeters to a few meters (30 cm to 8 m) and has an extension of a few meters to a few hundred meters (1 m to 500 m). These dykes underwent a deformation presented on the ground by boudinage and strike-slip faults shifted their architectures. These pegmatites are exclusively hosted in the Sarhlef Shale which is of the Upper Devonian age (Frasnian-Famennian), covers a large area and constitutes the central unit of the Jebilet [29]. It is anoxic sedimentation formed in a marine platform environment [39], composed mainly of sandstone-pelite with sometimes alternating sandstone and pelitic banks (Figure 3.a); at the top, the calcareous sedimentation does occur (Figure 3.b). In the study area, the host rock shows alternating levels of metapelite with andalusite and/or cordierite, and other unstained sandstone levels. This alternance is observed at small scale (centimetric) as well as at large scale (meter-size).

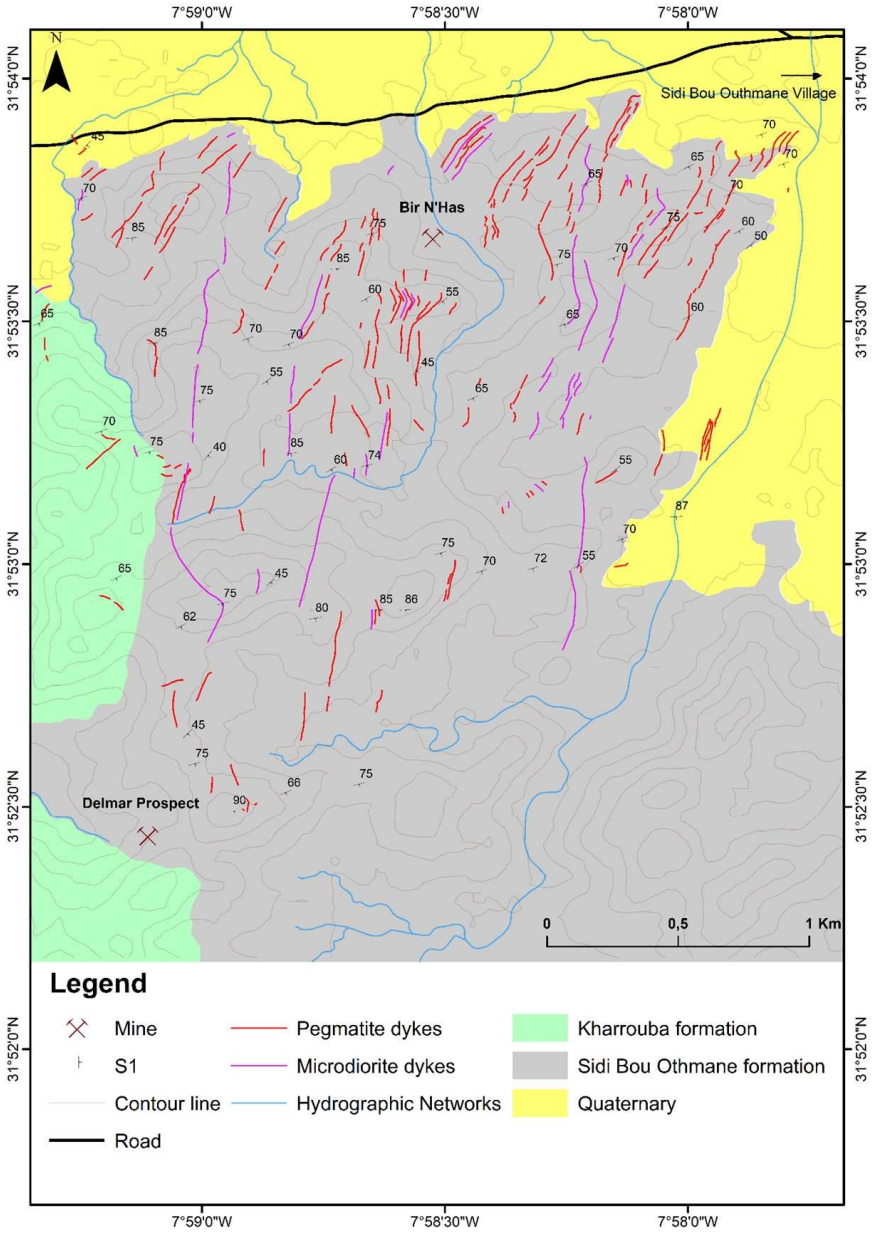

Preprints (www.preprints.org) | NOT PEER-REVIEWED | Posted: 25 December 2023 doi:10.20944/preprints202312.1793.v1

Figure 2. Simplified geological map showing the distribution of the pegmatites within the Sidi Bou Othmane area.

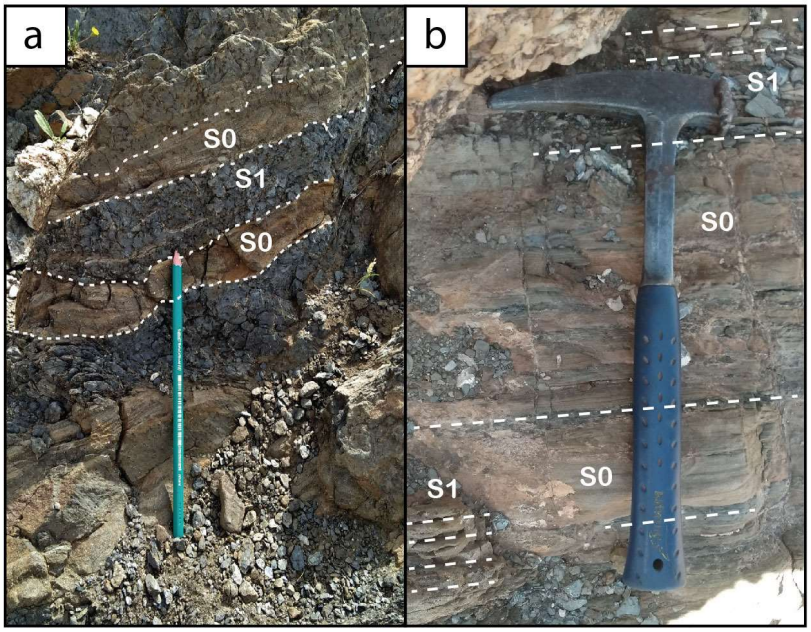

Figure 3. (a) The host rock shows alternating between metapelite and sandstone;**(b)** note the calcareous levels at the top (left). S0 is stratification and S1 is schistosity.

On the other hand, SBO pegmatites are mainly constituted by the association of quartz, albite, muscovite, and sometimes tourmaline and potassium-rich feldspar, (**Figure 4.a**, **b**). They are generally unzoned but, differently from what [20] reported, some zoned pegmatites have also been observed in the field. A zonation, which is quite clear both at large and small scale.

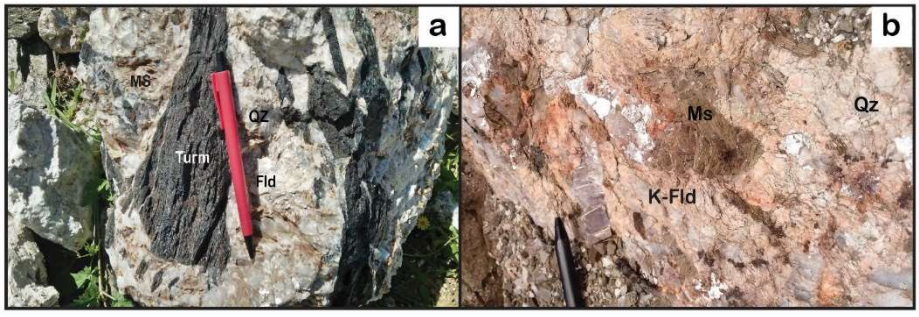

Figure 4. Field pictures showing the mineralogy of a pegmatite vein with tourmaline (Turm), muscovite (MS), quartz (QZ) and feldspar (Fld) (**a**), and (**b**) a pegmatite vein without Turm and MS-rich.

A general sequence of internal mineralogical zonation has been extracted, from the border to the core (**Figure 5**):

- the Border zone represents a thin layer of a few millimeters in contact with the host rock. Their mineralogy is essentially the same as that of the wall zone;
- the Wall zone is formed by quartz, feldspar (mainly albite, and, muscovite, and tourmaline of various size (i.e. from a few millimeters to centimeters);
- the Intermediate zone is composed of quartz and feldspar. This unit is characterized by a large increase in the crystal size;
- the Inner zone (core) is the internal part of the pegmatitic bodies, it is essentially constituted by massive quartz and is mainly a monomineralic part.

Preprints (www.preprints.org) | NOT PEER-REVIEWED | Posted: 25 December 2023 doi:10.20944/preprints202312.1793.v1

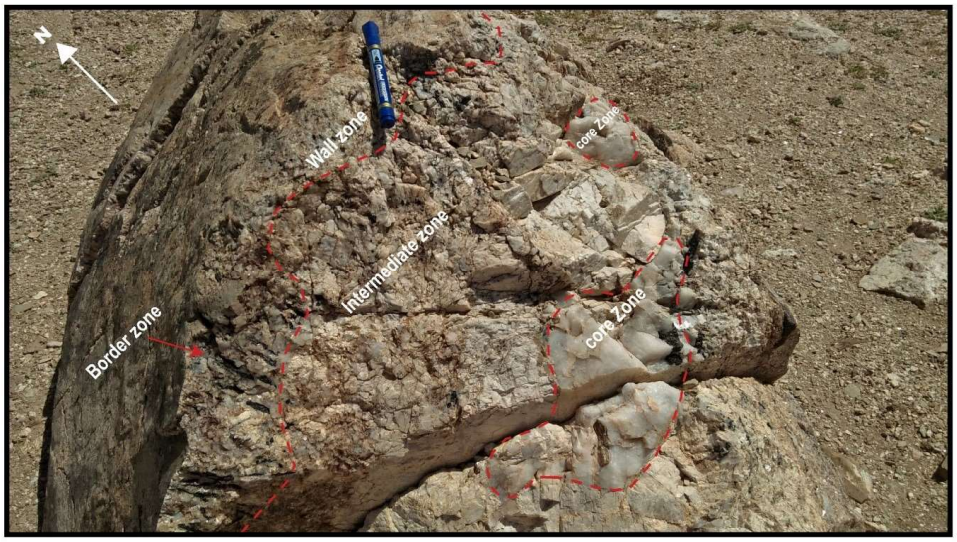

Figure 5. Field picture shows the zonation that has been observed in the pegmatite in Sidi Bou Othmane area.

4.2. Deformation and metamorphism

The central Jebilet of which SBO is a part has undergone an intense tectonic deformation with at least four phases (D1, D2, D3, D4), which resulted in the almost total disappearance of early structures (the stratification S0). This is the major compressive phase of the Hercynian cycle shows that the Hercynian orogeny stretched out between 330 and 250 Ma [34]. The deformation allowed the development of several structures. It is represented by the S1 schistosity, shear zones, boudins, and folds.

The analysis and study of these structures will allow us to establish a chronology between the different phases of deformation known at the time as well as the possible relationship between these phases.

4.2.1. Schistosity

The S1 schistosity is very apparent in all the facies. It is materialized by tight planes in the sandstone metapelites and less tight in the carbonate metapelites. At the scale of the study area, the schistosity trajectories show a direction that varies from N0 to N35, with a dominance of the N20 direction. They present a dip varying from 30° to 85° to the West, this schistosity is linked to a strong E-W compression.

On a more local scale, we note in some places an abrupt variation in the dip of the S1 schistosity towards the East, notably next to the pegmatite dykes. The directions of the S1 schistosity are almost N-S (between N0 and N20). The pole dip rosette shows a concentration of poles on the eastern side which means that the S1 dips to the west (**Figure 6**).

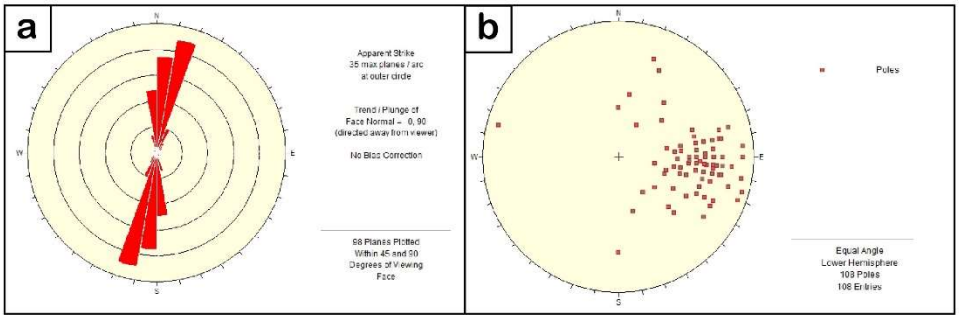

Figure 6. Structural features measured at the scale of (**a**) the outcrop directional rosette of the schistosity and (**b**) the pole dip rosette of fold.

Preprints (www.preprints.org) | NOT PEER-REVIEWED | Posted: 25 December 2023 doi:10.20944/preprints202312.1793.v1

4.2.2. Folding

The trajectories of S1, show that there is generally a great regularity in the direction and dip of the planes of S1, with a little variable direction from N0° to N30° and a variable dip (in the east the dip is westward, but in the western part of the study area the dip is eastward).

These results show that the SBO formations have undergone folding (P) that goes with the flow schistosity (S1). The folds of millimeter to centimeter sizes are highlighted by the folding of S1.

This can be clearly seen in the strike of some of the pegmatite veins (**Figure 7a**). During the major deformation, the more competent levels (pegmatites) undergo boudinage **(Figure 7b, c)**, along the planes of the schistosity, forming spindle-shaped crystallization tails at their edges (**Figure 7d, e**); this shows well that the setting of the pegmatites is syn to post-deformation. It is also remarkable the elongation of the small quartz veins which are intercalated in the schists. The elongation of these quartz veins is parallel to the deformation elongation axis X and perpendicular to the shortening axis Z **(Figure 7f)**.

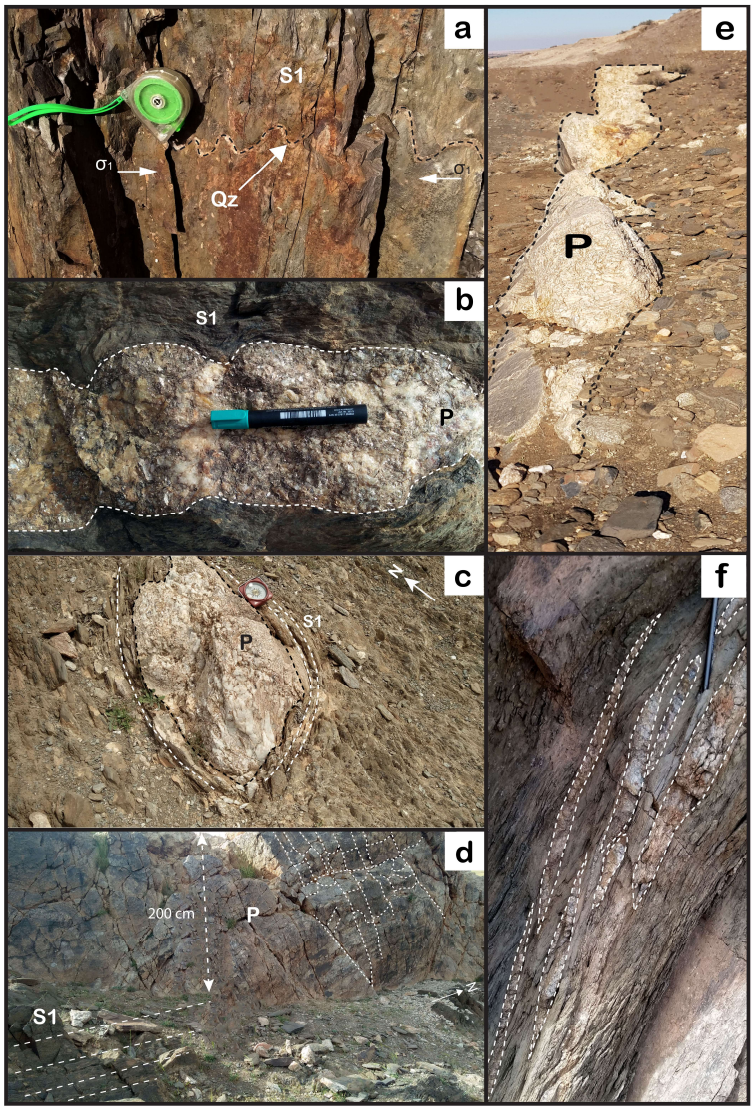

Figure 7. Field pictures showing (a)S1 schistosity folding, (b and c) boudinaged pegmatite dykes, (d) diaclases; (e) pegmatite boudinaged dike, (f)tension jointsin a pegmatite dyke (P: Pegmatite; S1: Schistosity).

Tension joints are evidence of the shearing that affected the central Jebilet (**Figure 7f**). The cracks related to this major phase have an average direction of N10 to N15 and they are centimetric to decimetric in size. The filling of these tension joints is generally by quartz, in response to E-W shear.

Preprints (www.preprints.org) | NOT PEER-REVIEWED | Posted: 25 December 2023 doi:10.20944/preprints202312.1793.v1

The brittle tectonics is materialized by a fracturing which affects essentially the pegmatite dykes and sometimes the quartz veins, but also at the level of the sandstone bars in the form of diaclases. The microdiorite veins and the quartz-carbonate veins are included in fractures linked to these brittle tectonics.

In the area of study, this tectonics is developed at a large extent, materialized essentially by decoupling, it is manifested by a lateral displacement of the magmatic veins (pegmatites; microdiorites), limestone bars, and quartz veins. These early quartz veins and the pegmatite veins are offset by faults of general direction N110 to N140.

4.3. Petrography

The petrographic investigation revealed that quartz, feldspar, plagioclase, , muscovite and tourmaline are common (Table 1) **(Figure 8a-f)** in the SBO rocks with some accessory minerals as zircon and garnet **(Figure 7a)**. Among the minerals present feldspar is the dominant mineral phase. Albite is the most common felsdspar s.l. By modal analysis albite constitutes most of the analyzed samples >47vol%, with the presence of the other terms like microcline and anorthite being less than 3%. Albite presents bands in the direction of elongation **(Figure 7c-f)**. It appears in the form of elongated rod-like sections, with sharp cleavages parallel and perpendicular to the elongation of the mineral. This mineral is very altered in illite and sericite (Figure 9c-f).

Quartz is the most abundant mineral after feldspar in SBO pegmatites and **(Figure 8 a-f)**. it is marked by patches of xenomorphic crystals, and it also occurs as inclusions in feldspar and muscovite. Also, another very striking criterion in quartz is the undulate extinction, chessboard patterns (**Figure 8e**) and triple points that indicate that the mineral underwent deformation.

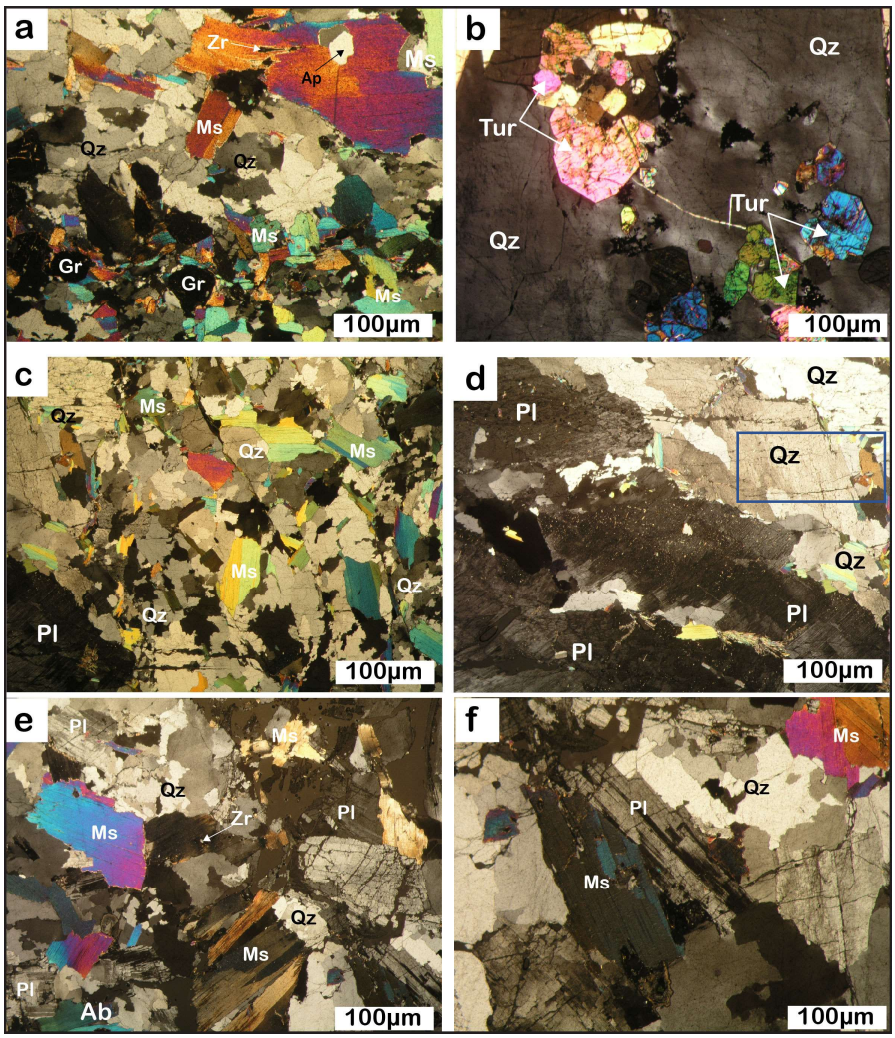

 doi:10.20944/preprints202312.1793.v1

Figure 8. Photomicrographs showing (***a***) large muscovite (Ms), albite (Ab) and quartz (Qz) crystals, garnet (Gr) and zircon (Zr); (***b***) large quartz with tourmaline (Tur); (***c***) and(***d)*** sheared area with plagioclase (Pl), quartz (Qz) and muscovite (Ms); (***e*** and ***f***) large patches of cataclastic plagioclase (Pl) (albite Ab) with and quartz (Qz), and muscovite (Ms).

Muscovite occurs as euhedral crystals, which are large elongated subautomorphic sheets or micaceous tablets with irregular contours (**Figure 8a**, **e**, **f**).

In some cases, muscovite is deformed showing a rolling extinction; this mineral can be observed either as gigantic minerals of centimetric size and as small inclusions within plagioclase. Muscovite sometimes shows a preferential orientation along the schistosity plane. Among micas, biotite occurs with tiny crystals.

Tourmaline is usually found both as basal sub-hedral and elongated sections. Irregular fractures may occur (Figure 8b).

Among the accessory mineral phases, it is worth noting the occurrence of garnetin some specimens (**Figure 8a**). Garnet is very rich in muscovite and tourmaline inclusions. Zircon is also present in many specimens (**Figure 8a**, **e**).

4.4. Whole rock geochemistry

Major, minor and trace element content, including REEs, have been used here to characterize the distinct geochemical characteristics of rock types. These geochemical data are presented in Table 2 and Table 3.

 doi:10.20944/preprints202312.1793.v1

Table 2. Major elements (wt%) of SBO pegmatite dykes. b.d.: Below detection limits.

Sample	SiO_2	Al_2O_3	Fe_2O_3	FeOtot	CaO	MgO	K_2O	MnO	TiO_2	P_2O_5	Na_2O	SO_3
SBO-01	77.04	14.3	0.48	0.432	0.25	b.d.	2.13	0.03	0.01	0.19	4.05	0.61
SBO-02	74.84	14.84	0.37	0.333	<0,10	b.d.	1.97	0.04	0.01	0.62	5.64	0.57
SBO-03	73.05	15.52	0.88	0.792	0.74	0.10	3.9	0.07	0.01	0.58	3.74	0.63
SBO-04	78.94	13.3	1.26	1.134	0.29	0.12	2	0.05	0.02	0.13	2.05	0.63
SBO-05	77.52	14.03	0.74	0.666	0.27	b.d.	3.7	0.03	0.01	0.16	0.90	0.65
SBO-06	72.51	16.11	0.99	0.891	0.72	b.d.	3.77	0.07	0.01	0.60	3.82	0.62
SBO-07	74.06	16.24	<0,10	b.d	0.21	b.d.	1.3	0.02	0.01	0.14	6.63	0.63
SBO-08	74.84	15.72	0.75	0.675	0.53	b.d.	3.55	0.17	0.02	0.36	0.96	0.60
SBO-09	75.41	15.25	0.95	0.855	0.50	b.d.	3.52	0.14	0.02	0.29	0.44	0.60
SBO-10	76.47	14.08	1.02	0.918	0.54	0.1	3.83	0.07	0.04	0.36	0.16	0.62
SBO-11	72.82	15.63	0.34	0.306	0.73	b.d.	3.23	0.10	0.01	0.76	5.10	0.69
SBO-12	73.6	16.51	0.5	0.45	0.29	b.d.	5.27	0.03	0.01	0.23	0.24	0.61
SBO-13	71.09	19.45	<0,10	b.d	0.33	b.d.	4.96	0.02	0.01	0.15	0.33	0.68
SBO-14	73.57	17.46	0.23	0.207	0.18	b.d.	4.50	0.02	0.01	0.12	0.55	0.70
SBO-15	77.07	13.94	0.22	0.198	0.3	b.d.	0.71	0.03	0.01	0.38	5.76	0.62
SBO-16	74.97	14.08	0.6	0.54	1.27	b.d.	1.93	0.14	0.01	0.89	4.23	0.62
SBO-17	69.91	18.71	0.97	0.873	1.14	0.16	3.97	0.03	0.07	0.8	0.42	0.63
SBO-18	72.04	17.45	0.39	0.351	0.70	b.d.	2.52	0.07	0.02	0.59	3.73	0.60
SBO-19	72.6	17.93	0.7	0.63	0.37	b.d	4.00	0.04	0.02	0.23	0.72	0.64
SBO-20	74.79	14.68	0.82	0.738	0.62	b.d	2.04	0.22	0.01	0.88	4.26	0.66
SBO-21	80.21	12.04	0.64	0.576	0.49	v	0.42	0.18	0.01	0.21	4.94	0.61
SBO-22	74.83	14.66	4.21	3.789	0.46	0.10	0.35	0.09	0.03	0.25	3.84	0.71
SBO-23	69.47	18.29	1.39	1.251	1.11	0.63	3.12	0.08	0.22	0.41	0.36	0.51
SBO-24	74.47	16.06	2.35	2.115	0.43	0.23	0.81	0.05	0.03	0.20	4.41	0.65

 doi:10.20944/preprints202312.1793.v1

SBO-25	74.05	15.9	1.62	1.458	0.56	b.d	1.78	0.05	0.01	0.24	4.02	0.61
SBO-26	76.01	15.59	1.16	1.044	0.31	b.d	1.38	0.04	0.01	0.21	4.11	0.63

Table 3. Minor, minor trace and rare earth elements of SBO pegmatite dykes. Contents are expressed as mg/kg., n.d.= not detected.

Sample	Ti	K	As	P	Ba	Be	Bi	Cd	Co	Cr	Cu	Li	Mo	Nb	Ni	Pb	Rb	Sb	Sc	Se	Sn	Sr	Th	U	V	Y	Zn	Zr	La	Ce	Pr	Nd	Sm	Eu	Gd	Tb	Dy	Ho	Er	Tm	Yb	Lu	PF	Cl
SBO-01	59.951	45	172	829.16	29.3	6.3	15.8	4.8	n.d.	108.3	9.3	143	6.1	14.6	6.7	n.d.	333.3	31.3	7	n.d.	22.7	51.4	0.5	1.1	2.1	0.6	49.6	9.1	1	1.3	0.3	0.8	0.6	0.1	0.4	0	0.2	0.1	0.1	0.1	0.1	0.1	0.96	465.3
SBO-02	59.951	42	87	2705.68	22.7	10.4	14.1	1.9	n.d.	35	5.6	98.7	n.d.	37.8	n.d.	n.d.	359.9	2.2	5.7	n.d.	44.3	85.3	1.3	4	3	0.8	39.4	17.7	1.2	1.9	0.3	0.9	0.7	0	0.5	0	0.3	0.1	0.1	0.1	0.1	0.1	1.01	310.2
SBO-03	59.951	83	93	2531.12	101.8	5.4	12.2	2.3	n.d.	116	6.4	141.7	1.9	44.1	1.1	n.d.	759.5	10.5	5.9	n.d.	28	135.7	1.3	1.5	3	2	69.2	13.7	1.1	1.8	0.4	1.6	0.9	0.3	0.8	0.1	0.5	0.1	0.2	0.1	0.2	0.1	0.93	443.1
SBO-04	119.902	42	77	567.32	17.1	4.3	4.5	0.9	n.d.	57.9	7	130.6	n.d.	n.d.	11.5	n.d.	338.5	n.d.	6.2	n.d.	27	39.8	0.7	0.5	5.7	0.8	36.8	9.4	1	1.5	0.3	0.8	0.6	0	0.5	0	0.2	0.1	0.2	0.1	0.1	0.1	1.08	819.8
SBO-05	59.951	79	74	698.24	35.5	6.4	20	1.9	n.d.	176.6	8	208.9	1.3	46.7	<0.1	n.d.	1201	n.d.	5.2	n.d.	107.4	90.8	0.8	1.2	1.3	0.9	38.3	11.4	1.2	1.2	0.3	0.9	0.7	0.1	0.6	0.1	0.5	0.1	0.2	0.1	0.1	0.1	1.49	886.3
SBO-06	59.951	80	101	2618.4	92.1	5.2	18.5	2.8	n.d.	111.3	4.7	128.4	n.d.	43.7	n.d.	n.d.	716.6	n.d.	5.6	2.9	27.9	126.5	1.3	1.6	2.5	1.9	62	12.7	1.1	2.1	0.4	1.6	0.9	0.3	0.8	0.1	0.7	0.1	0.2	0.1	0.2	0.1	0.82	576.1
SBO-07	59.951	28	87	610.96	24.8	5.5	15.4	1.2	47.3	90.4	9.3	193.4	4.5	3.7	9.5	n.d.	446	5	4.6	4.4	31.4	50.7	0.5	0.1	1.7	0.5	19.1	6.2	0.8	0.9	0.2	0.7	0.6	0.1	0.4	0	0.2	0.1	0.1	0.1	0.1	0.1	0.72	310.2
SBO-08	119.902	75	57	1571.04	58.7	4.6	22.2	1.5	n.d.	39.2	3.5	170.5	3.8	n.d.	2.4	n.d.	408.7	1.4	6.6	n.d.	27.1	50.4	1.8	5.1	4.2	5	32.9	17	1.7	3.5	0.6	1.8	1	0.2	0.9	0.2	1	0.2	0.5	0.2	0.7	0.1	1.64	731.2
SBO-09	119.902	75	46	1265.56	34.7	3.9	n.d.	1.7	n.d.	174.2	5.1	155.1	n.d.	12.1	10.8	n.d.	435.9	9.7	7.1	n.d.	24.3	44	0.8	1.6	4.1	1.9	39.1	11.9	1.1	2.1	0.4	1.1	0.7	0.2	0.6	0.1	0.5	0.1	0.3	0.1	0.3	0.1	1.94	775.5
SBO-10	239.804	81	62	1571.04	51.1	3.6	n.d.	2.6	n.d.	48.2	5.7	191.6	n.d.	9.8	<0.1	n.d.	471.1	14.2	7.5	n.d.	41.5	44.7	1.4	3.5	3.9	3.5	49.3	17.9	1.6	3.1	0.5	1.6	0.9	0.1	0.8	0.1	0.7	0.2	0.4	0.2	0.6	0.1	1.76	753.3
SBO-11	59.951	69	205	3316.64	13.4	6.8	n.d.	5	n.d.	38.5	6.9	140.4	7.1	20.8	9.8	n.d.	847.4	n.d.	5.6	n.d.	14.2	131	0.7	1.6	3.2	0.8	59.2	15.8	0.9	1.1	0.3	0.7	0.6	0.1	0.5	0	0.2	0.1	0.1	0.1	0.1	0.1	0.67	421
SBO-12	59.951	112	72	1003.72	151.9	7.8	20.6	1.6	n.d.	37	4.3		2.8	44.2	3.7	n.d.	868.2	10.5	5.2	n.d.	50.4	53.4	0.8	1.5	2.8	0.9	30.4	17.7	1	1.4	0.3	0.8	0.6	0.2	0.5	0	0.3	0.1	0.2	0.1	0.1	0.1	2.36	531.8
SBO-13	59.951	105	209	654.6	33.2	8	18.5	5.9	200.3	83.7	8.7	153.7	7.2	49.6	19	n.d.	1571	<0.1	4	<0.1	102.6	48.6	0.5	1.3	5.1	0.7	59.5	66.8	0.9	1	0.2	0.7	0.6	0.1	0.4	0	0.2	0.1	0.1	0.1	0.1	0.1	2.47	265.9
SBO-14	59.951	96	201	523.68	46.7	4.9	13.8	5.2	17.2	158.6	8.3	39.4	n.d.	74.6	16.9	n.d.	1466	n.d.	4	0.9	71.2	66.8	0.6	1.7	3.2	0.7	14.8	37.5	0.7	0.6	0.2	0.6	0.6	0.1	0.4	0	0.2	0.1	0.1	0.1	0.1	0.1	2.31	332.3
SBO-15	59.951	15	109	1658.32	22.7	3.3	21.5	2.1	n.d.	164.2	8	19.3	10.7	190	10.2	16.7	272.8	16.7	4.8	n.d.	19.8	80.3	3.3	1.6	0.8	2.6	22	13.7	1.4	3.1	0.5	2.1	1.1	0.2	1	0.1	0.7	0.1	0.3	0.1	0.2	0.1	0.66	841.9
SBO-16	59.951	41	115	3883.96	26.9	8.6	0.9	2.9	n.d.	34.3	7.6	247.9	2.6	36.1	9.3	n.d.	700	5	6.2	5	51.4	86.2	1.1	2.5	2.8	3.9	109.6	15.4	2.3	3.7	0.6	2.6	1.4	0.9	1.5	0.2	0.8	0.1	0.3	0.1	0.2	0.1	1.54	398.8
SBO-17	419.657	84	46	3491.2	154.3	3.9	n.d.	0.6	n.d.	50.1	6.4	119.3	1.3	33.4	20.9	n.d.	585.8	1.9	4.8	3.9	62.9	75.9	1.2	1.3	14.1	2.6	25.7	10.6	2.9	5.8	0.8	3	1.1	0.7	0.9	0.1	0.6	0.2	0.4	0.1	0.3	0.1	2.34	797.6
SBO-18	119.902	54	65	2574.76	46.9	7.9	9.5	1	n.d.	132.8	3.4	38.8	1.2	8.5	25.5	n.d.	385.2	n.d.	3.6	n.d.	26.5	94.7	3.6	3.3	5.4	5.9	24.4	13.6	2.2	3.8	0.6	2.3	1.5	0.3	1.6	0.3	1.6	0.2	0.4	0.1	0.3	0.1	1.74	841.9
SBO-19	119.902	85	66	1003.72	83.9	9.4	n.d.	2.5	n.d.	50	4.2	71.2	n.d.	35.2	0.2	n.d.	842.5	21.1	5.2	n.d.	41.6	52.7	1.7	0.8	3.9	1.3	25.7	8.7	1.2	1.5	0.3	1	0.7	0.2	0.6	0.1	0.4	0.1	0.2	0.1	0.1	0.1	2.07	598.2
SBO-20	59.951	43	42	3840.32	16.5	4.5	13.5	3.9	n.d.	38.7	4.1	141.7	n.d.	21.7	1.1	7.7	716.6	12.1	5.9	n.d.	22.4	116.8	1.1	10.9	2.2	1.2	206.8	25	0.9	1.1	0.3	0.8	0.6	0	0.5	0	0.3	0.1	0.2	0.1	0.2	0.1	0.9	288
SBO-21	59.951	9	112	916.44	10	3.8	n.d.	2.5	n.d.	145.1	3.3	16.9	n.d.	n.d.	16.4	n.d.	28.6	15.1	6.6	21.4	0.6	38.1	1.3	9.2	<0.1	5.6	14	20.3	2	4.1	0.6	1.9	1	0	0.9	0.1	1	0.3	0.6	0.2	1.1	0.2	0.22	310.2
SBO-22	179.853	7	345	1091	20.8	3.6	18.3	8.9	n.d.	231.1	11.5	44.3	13.7	n.d.	11.8	n.d.	72.4	n.d.	5.9	n.d.	6	69.3	1.5	2.7	5.8	2.5	117.4	17.5	1.5	2.3	0.4	1.3	0.9	0.1	0.7	0.1	0.6	0.1	0.3	0.1	0.4	0.1	0.39	332.3
SBO-23	1.318.922	66	138	1789.24	551.5	10	n.d.	2.7	n.d.	59.3	8.2	1893	1.1	48	12.2	n.d.	1714	3	9.6	14.5	415.7	164.3	5.5	1.3	63.9	8.7	107.2	33.1	15.2	29	3.4	12.5	2.6	1.2	2.5	0.3	1.8	0.4	1	0.2	0.9	0.2	3.57	398.8

Preprints (www.preprints.org) | NOT PEER-REVIEWED | Posted: 25 December 2023 doi:10.20944/preprints202312.1793.v1

SBO-24	179.853	17	122	872.8	18.6	3.3	21	2.9	n.d.	206.8	23.6	36.3	0.7	<0.1	18.7	n.d.	84.99	n.d.	6.1	n.d.	2.5	40.5	0.8	1.2	3.2	1.7	66.9	18.2	1.6	3	0.5	1.5	0.8	0.1	0.6	0.1	0.3	0.1	0.2	0.1	0.3	0.1	0.4	310.2
SBO-25	59.951	38	121	1047.36	12.7	3.7	11	2.9	45.8	51.9	7.6	74.7	5.4	7.3	19.7	n.d.	248.4	16.7	7.1	n.d.	16.8	50.7	3.7	2.2	6.3	1.3	52.9	15.9	1.5	5.3	0.5	1.6	1	0.1	0.7	0.1	0.4	0.1	0.2	0.1	0.4	0.1	1.12	709
SBO-26	59.951	29	32	916.44	9.1	4.5	16.4	0.5	n.d.	145.8	5.6	176.6	4.9	1	<0.1	n.d.		9.4	5.2	n.d.	20.3	48.1	1.1	0.5	1.4	0.8	41.5	7.7	0.8	1.3	0.2	0.7	0.6	0	0.5	0	0.2	0.1	0.1	0.1	0.1	0.1	0.76	753.3

Table 4. CIPW norm Holacher calculation for Sidi Bou Othmane Pegmatites.

Minerals Weight %	SBO-01	SBO-02	SBO-03	SBO-04	SBO-05	SBO-06	SBO-07	SBO-08	SBO-09	SBO-10	SBO-11	SBO-12	SBO-13	SBO-14
Quartz	52..09	54..38	33..77	52..42	45..22	45..69	53..23	51..78	36..45	38..84	36..36	33..24	44..69	47..60
Plagioclase	0..00	0..20	38..63	28.52	32.24	35.36	0.00	38.86	43.99	27.52	31.30	52.13	31.72	33.06
Orthoclase	29.31	29.31	19.09	2.07	11.41	12.59	31.14	2.48	11.64	23.05	18.44	7.68	12.06	4.79
Corundum	14.08	12.03	4.62	8.62	5.63	4.24	10.81	3.85	4.16	5.95	8.31	4.67	6.27	8.76
Hypersthene	0.02	0.20	0.28	3.60	0.73	0.41	0.44	0.84	1.35	0.80	0.92	0.11	1.07	2.30
Ilmenite	0.02	0.02	0.02	0.06	0.02	0.02	0.02	0.02	0.02	0.02	0.42	0.04	0.02	0.06
Magnetite	0.00	0.33	0.49	6.10	0.87	0.70	0.72	0.93	0.54	1.15	2.02	0.00	1.19	3.41
Apatite	0.35	0.28	1.76	0.58	2.06	0.44	0.53	0.49	1.44	1.34	0.95	0.32	2.04	0.46
Zircon	0.01	0.01	0.00	0.00	0.00	0.00	0.00	0.00	0.00	0.00	0.00	0.00	0.00	0.00
Chromite	0.00	0.03	0.01	0.04	0.01	0.03	0.01	0.03	0.01	0.03	0.01	0.01	0.01	0.01
Anhydrite	1.16	0.00	0.00	0.00	0.00	0.00	0.00	0.00	0.00	0.00	0.00	0.00	0.00	0.00
Na2SO4	0.00	1.24	1.22	1.26	1.10	1.08	1.08	1.08	1.01	1.12	0.90	1.12	1.17	1.15
Total	97.04	98.03	99.89	103.27	99.29	100.56	97.98	100.36	100.61	99.82	99.63	99.32	100.24	101.60
Fe3+/(Total Fe) in rock	0.0	49.6	49.7	50.0	50.0	50.1	50.0	49.8	36.5	49.0	50.0	0.0	49.9	49.9
Ca/(Ca+Na) in rock	100.0	15.3	7.3	6.2	14.2	14.8	40.0	5.2	0.0	0.0	14.1	1.7	7.4	0.6
Ca/(Ca+Na) in plagioclase	0.0	65.2	0.0	2.2	1.5	13.7	0.0	2.6	0.0	0.0	9.1	0.3	0.0	0.0
Differentiation Index	81.4	83.9	91.5	83.0	88.9	93.6	84.4	93.1	92.1	89.4	86.1	93.1	88.5	85.5
Calculated density. g/cc	2.76	2.74	2.68	2.84	2.71	2.69	2.74	2.69	2.69	2.70	2.75	2.67	2.72	2.79
Calculated liquid density	2.37	2.36	2.36	2.44	2.37	2.36	2.36	2.35	2.36	2.37	2.41	2.36	2.37	2.40
Calculated viscosity. dry	12.4	12.8	10.2	9.9	11.7	12.2	12.8	13.8	11.0	10.8	9.1	10.8	11.5	10.6

Calculated viscosity. wet	9.0	8.9	7.3	7.3	7.9	8.3	8.9	8.6	7.7	7.7	7.1	7.7	7.9	7.7
Estimated liquidus temp.	783	755	791	802	746	726	750	665	755	779	853	763	755	784
Estimated H2O content	4.13	4.45	4.04	3.91	4.53	4.76	4.49	5.43	4.42	4.17	3.32	4.34	4.43	4.10

Table 4. CIPW norm Holacher calculation for Sidi Bou Othmane Pegmatites.

Minerals Weight %	**SBO-15**	**SBO-16**	**SBO-17**	**SBO-18**	**SBO-19**	**SBO-20**	**SBO-21**	**SBO-22**	**SBO-23**	**SBO-24**	**SBO-25**	**SBO-26**	**SBO-28**	**SBO-27**
Quartz	45.70	47.59	61.27	60.62	61.25	43.55	57.83	61.10	53.90	43.22	38.04	42.07	20.95	97.68
Plagioclase	30.61	30.84	13.81	3.68	0.00	44.68	4.52	0.95	0.36	0.00	27.75	28.26	39.54	0.00
Orthoclase	10.52	10.52	11.82	21.87	22.63	4.20	20.98	20.80	23.46	9.35	23.64	16.37	24.29	0.00
Corundum	7.92	7.63	8.35	9.25	9.93	4.49	10.94	11.26	14.34	0.00	8.14	7.62	0.08	0.00
Hypersthene	1.41	0.99	1.47	0.63	1.15	0.21	0.89	0.42	1.13	0.00	0.61	0.91	9.23	0.00
Ilmenite	0.02	0.02	0.04	0.02	0.08	0.02	0.04	0.04	0.13	0.57	0.04	0.02	1.46	0.02
Magnetite	2.35	1.68	1.83	1.07	1.48	0.32	1.09	1.23	1.41	0.00	1.01	1.44	8.02	0.00
Apatite	0.56	0.49	0.30	0.37	0.83	0.88	0.83	0.67	1.85	0.00	0.53	1.39	0.44	0.09
Zircon	0.00	0.00	0.00	0.00	0.00	0.00	0.00	0.00	0.00	0.00	0.00	0.00	0.01	0.00
Chromite	0.01	0.03	0.01	0.04	0.01	0.03	0.01	0.04	0.01	0.00	0.01	0.03	0.01	0.00
Anhydrite	0.00	0.00	0.00	0.00	0.18	0.00	0.00	0.30	0.24	1.06	0.00	0.00	0.00	0.00
Na2SO4	1.08	1.12	1.12	1.15	0.91	1.10	1.06	0.75	0.87	0.00	1.14	1.10	0.28	0.00
Total	100.18	100.91	100.02	98.70	98.45	99.48	98.19	97.56	97.70	98.56	100.91	99.21	104.31	98.16
Fe3+/(Total Fe) in rock	50.0	50.1	45.8	49.8	49.9	49.7	50.2	60.5	50.1	50.1	50.0	50.0	50.0	0.0
Mg/(Mg+Total Fe) in rock	0.0	0.0	0.0	0.0	8.8	0.0	0.0	0.0	14.1	0.0	0.0	0.0	29.4	0.0
Mg/(Mg+Fe2+) in rock	0.0	0.0	0.0	0.0	16.2	0.0	0.0	0.0	24.7	0.0	0.0	0.0	45.5	0.0
Mg/(Mg+Fe2+) in silicates	0.0	0.0	0.0	0.0	26.6	0.0	0.0	0.0	41.8	0.0	0.0	0.0	69.0	0.0
Ca/(Ca+Na) in rock	5.6	4.0	7.3	14.2	65.1	2.8	23.4	38.6	60.0	9.4	5.2	9.4	44.7	100.0
Ca/(Ca+Na) in plagioclase	1.8	0.6	4.0	8.3	0.0	0.0	6.8	0.0	0.0	0.0	1.3	0.0	44.7	0.0
Differentiation IndexI would avoid this part. otherwise we	86.8	89.0	86.9	86.2	83.9	92.4	83.3	82.9	77.7	85.7	89.4	86.7	84.8	97.7

 doi:10.20944/preprints202312.1793.v1

explain the software in a detailed manner														
Calculated density. g/cc	2.75	2.73	2.75	2.74	2.76	2.68	2.76	2.76	2.80	2.73	2.72	2.73	2.82	2.65
Calculated liquid density	2.39	2.37	2.36	2.35	2.37	2.35	2.37	2.36	2.40	2.37	2.38	2.38	2.53	2.23
Calculated viscosity. dry	11.0	11.7	14.2	14.5	14.2	12.6	13.3	14.1	11.0	11.0	10.1	10.6	5.2	25.6
Calculated viscosity. wet	7.8	8.1	9.1	9.3	9.2	8.3	9.0	9.3	8.2	8.0	7.5	7.7	4.6	5.9
Estimated liquidus temp.	775	749	683	691	703	707	733	713	819		811	789	1002	303
Estimated H2O content	4.20	4.49	5.23	5.16	5.02	4.97	4.68	4.90	3.71		3.79	4.04	1.76	7.65

Preprints (www.preprints.org) | NOT PEER-REVIEWED | Posted: 25 December 2023 doi:10.20944/preprints202312.1793.v1

Table 5. CIPW norm calculation for SBO Pegmatites from maximum to minimum Na2O contents.

	SBO-PG7	SBO-PG12
Q	30.5	67.0
A	7.7	7.7
P	56.2	2
F	0.0	0.0
Total	100	100

The geochemical data of the SBO pegmatites samples show a wide range of major elements compositions with silica SiO_2 contents ranging from 69.47 to 80.21 wt.%. Al_2O_3 contents are generally high ranging from 12.04 to 19.45 wt.%, on the other hand, the other oxides are lower: $Na_2O \leq 5.76$; $K_2O \leq 5.27$ wt.%; $Fe_2O_3 \leq 5.53$, $FeO \leq 4.98$ wt.%; $MgO \leq 2.33$ and $TiO_2 \leq 0.77$ wt.%, $CaO \leq 3.86$ %, $MnO \leq 0.22$ wt.%, $P_2O_5 \leq 0.89$ wt.%. The Loss On Ignition (L.O.I.) shows values between 0.22 and 3.57 wt.%.

As far as the minor and trace elements analyzed from the pegmatite, Sr ranges between 38 and 164 mg/kg. The compatible elements, Ni (0-25.50ppm) and Cr (25-231 mg/kg) have low concentrations to high concentration. In most samples, the low concentrations of these compatible elements suggest that the materials that formed the pegmatite are probably derived from a depleted source.

Zr values are between 6 and 66 ppm and are related to the accessory zircon, which is the main mineral phase in which this element is concentrated. Ba concentration ranges from 9 to 551 ppm. The Ba is mainly detected in biotite and has a high affinity for potassium feldspar, in substitution to K [40]. Rb contents are relatively high, up to 1714 ppm; this element is generally incorporated in minerals such as biotite and potassium feldspar.

Furthermore, Ta and Nb contents range respectively from 0.8 to 4.2 mg/kg, 0 and 190 mg/kg. Li and Cs values are comprised respectively between 2.3 and 1893 mg/kg and 0.2to 277 mg/kg. Sn values reach 415 mg/kg. The concentrations of Nb, Ta, Sn, and Cs are relatively high and indicate enrichment within these rocks, Li reach the highest concentrations among trace elements. This can be explained by the higher proportion of recycled waste and an enriched source.

The sums of the concentrations of REE of SBO pegmatites range from .3.9 to 70 mg/kg which is lower compared to the international range (250–270 mg/kg) of Herman, 1970 [41]. The depletion of REEs has been attributed to various processes including magmatic differentiation [42], hydrothermal leaching [43], and or a combination of both. The sum of light rare earth element (ΣLREE) and the sum of heavy rare earth element (ΣHREE) concentration values for the pegmatite samples vary within the range of1.1–151 mg/kg and 0.6-13.30 mg/kg, respectively. Meanwhile, the La/Lu ratios vary from 9 to 76. The spectra also show slight negative or positive Eu anomalies with Eu/Eu* values ranging from 0.2 to 3.2. These anomalies are related to plagioclase fractionation.

The major and minor elements are plot into the Harker diagrams for oxides to determine their compatibility or relationship with silica. From the Harker diagram for oxides versus SiO_2 (**Figure 9**), it can be deduced that only Al_2O_3, shows a clear negative correlation with SiO_2. As SiO_2 increases, Al_2O_3, CaO, and Fe_2O_3 decrease, which would be related to tourmaline fractionation. Al_2O_3 and K_2O decrease with increasing SiO_2, which would be related to the formation of feldspars and muscovite. The dispersion of Na_2O contents in the analyzed samples may be mainly related to their mobility, indeed, two groups of samples can be distinguished for the same SiO_2 values, which would be related to the albite richness, while the variation of P_2O_5 would be related to the late apatite fractionation.

Preprints (www.preprints.org) | NOT PEER-REVIEWED | Posted: 25 December 2023 doi:10.20944/preprints202312.1793.v1

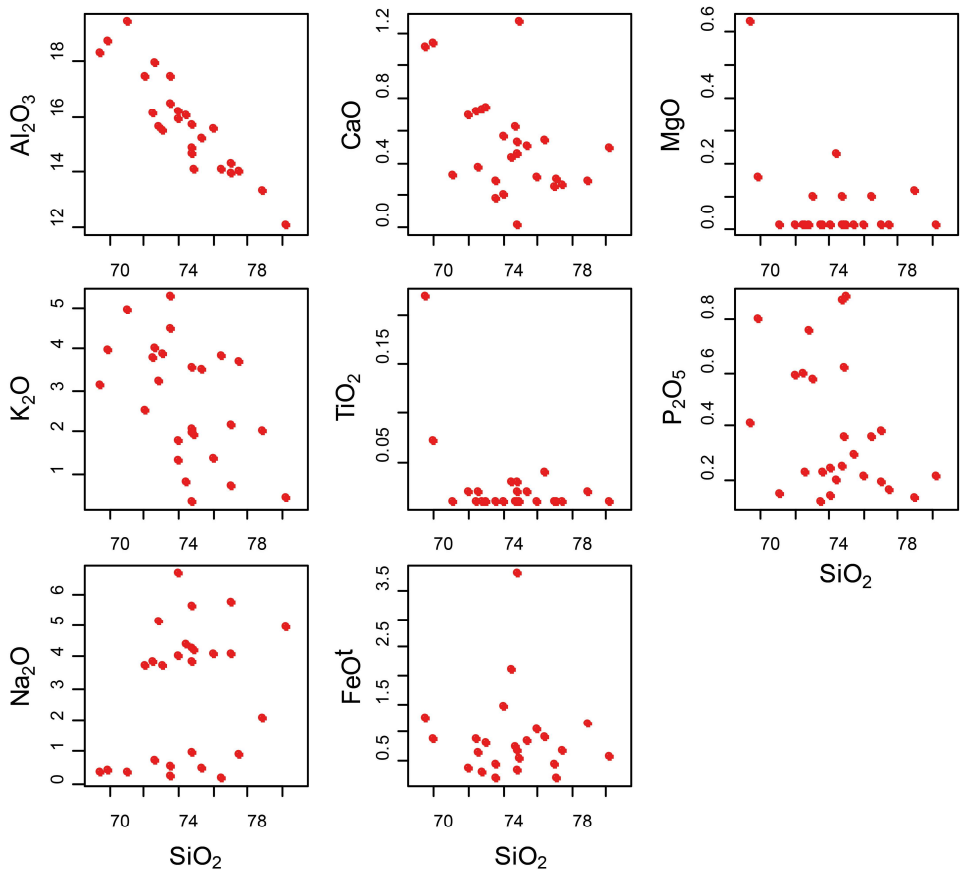

Figure 9. Binary variation diagrams showing major elements versus SiO_2 (wt%) of SBO pegmatites.

On the other hand, trace elements show a strong dispersion (**Figure 10**), thus, we note a very weak negative correlation between silica and Rb, Sr, Y and Zr, and even less evident with Ba, Ce, La and Ni.

Preprints (www.preprints.org) | NOT PEER-REVIEWED | Posted: 25 December 2023 doi:10.20944/preprints202312.1793.v1

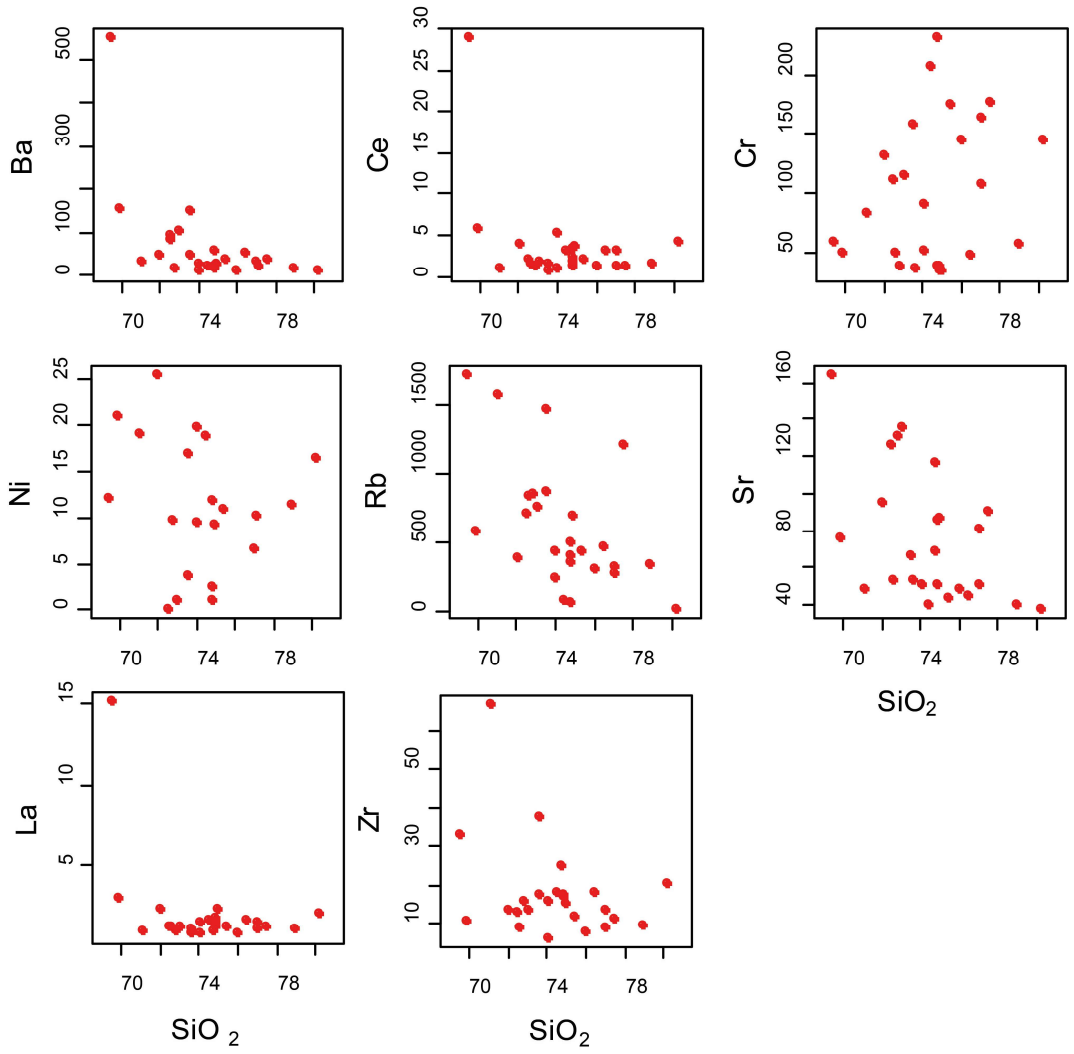

Figure 10. Binary variation diagrams showing trace elements versus SiO2 (wt%) of SBO pegmatites.

5. Discussion

5.1. Geochemical characteristics of the SBO pegmatites

5.1.1. Major elements

The results of geochemical analysis were plotted on a series of diagrams to determine the magmatic characteristics of SBO pegmatites. On the binary (Na_2O+K_2O) vs. SiO_2 diagram of Middlemost et al., [44], all samples plot within the granite field (**Figure 11**).

Preprints (www.preprints.org) | NOT PEER-REVIEWED | Posted: 25 December 2023 doi:10.20944/preprints202312.1793.v1

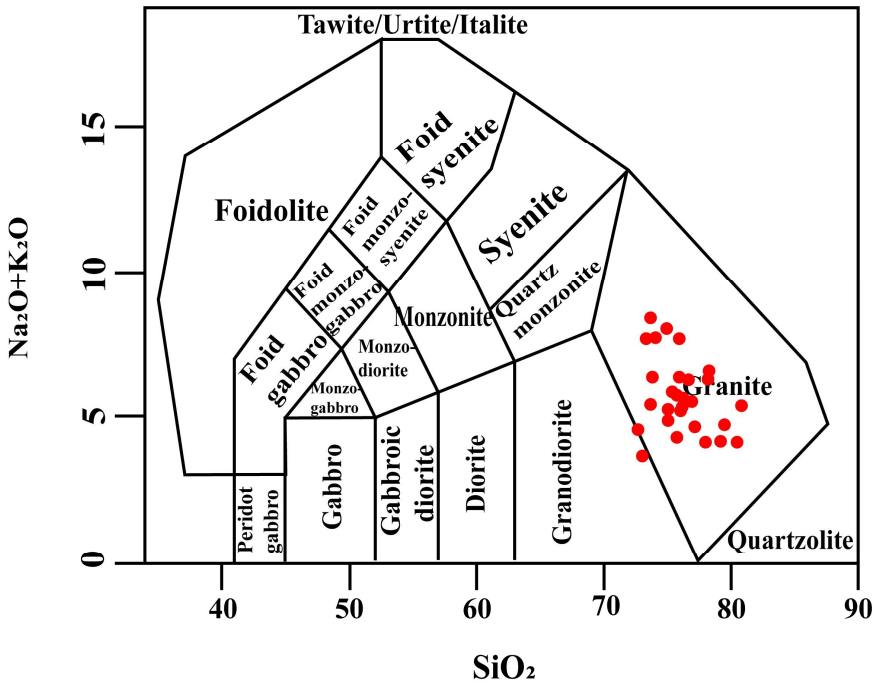

Figure 11. Classification diagrams of (SBO) pegmatite TAS diagram (Total Alkalis versus Silica after Middlemost et al., [44]. Please check the correct reference to diagram.

In the A/NK vs A/CNK diagram [45], which designates respectively: Al_2O_3/ (Na_2O+K_2O); Al_2O_3/ ($CaO+Na_2O+K_2O$), all samples show ratios of A/CNK and A/NK well above 1, reflecting the excess of alumina over Ca, Na and K. These rocks are therefore peraluminous (**Figure 12**), and this aluminum richness is indeed reflected in the mineralogy by the presence of muscovite together with feldspar, and tourmaline. It is also noted that excess Al_2O_3 is found as CIPW normative corundum in many pegmatite samples up to 12.8 wt.% (Table 4).

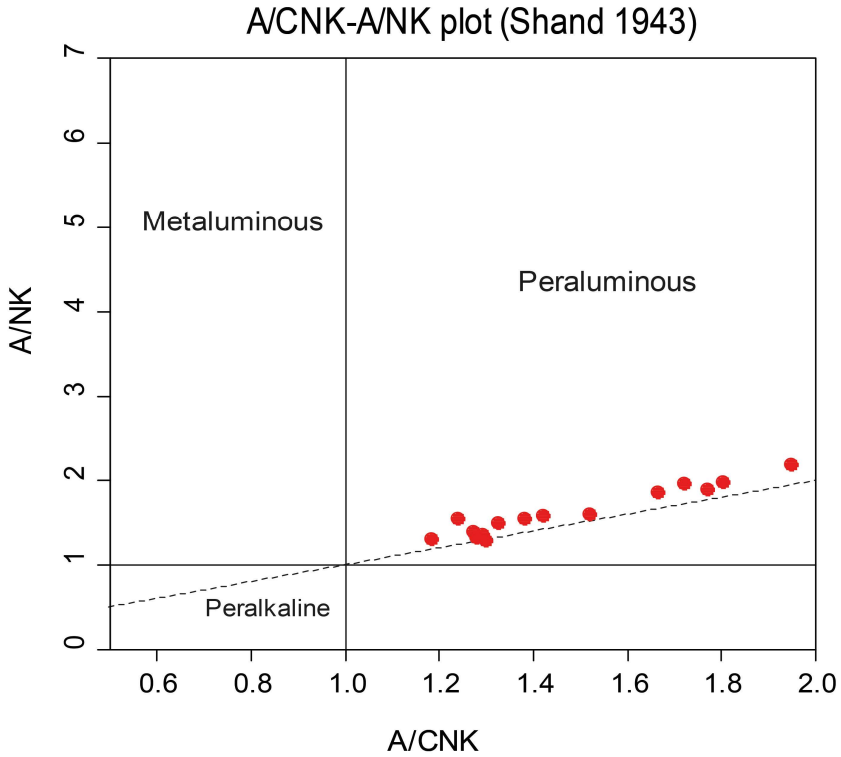

Figure 12. Classification diagrams. A/NK versus A/CNK diagram after Maniar et al. [45]; Al2O3/Cao+Na2O+K2O versus SiO2 after White et al. [46].

Preprints (www.preprints.org) | NOT PEER-REVIEWED | Posted: 25 December 2023 doi:10.20944/preprints202312.1793.v1

The AFM diagram after Irvine [47], shows calc-alcaline serie for SBO pegmatites (**Figure 13**).

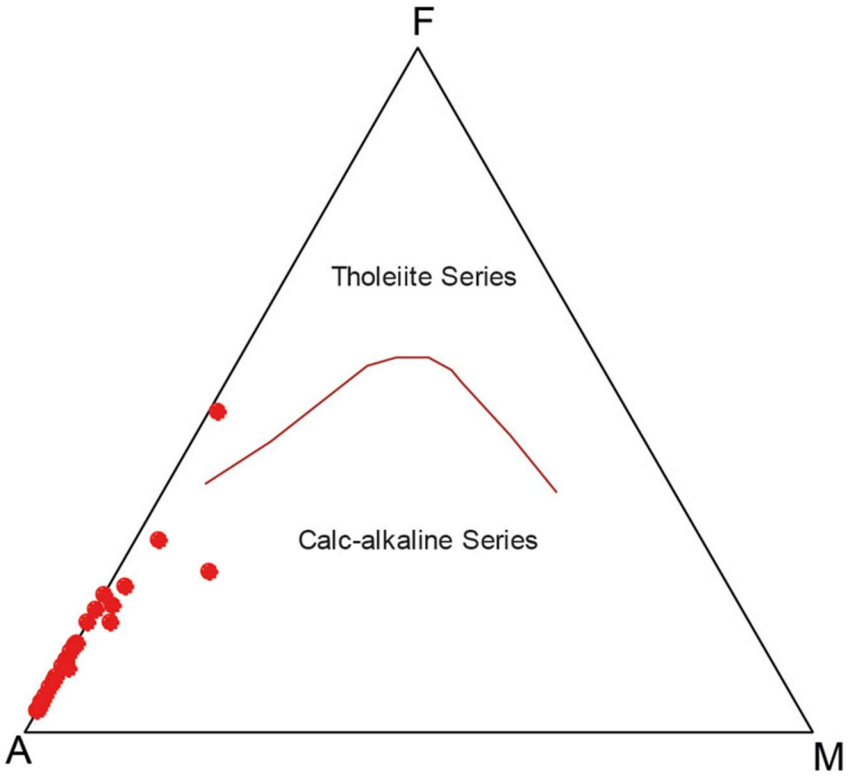

Figure 13. AFM diagram after Irvine et al. [47].

On the other hand, peraluminous granitic rocks, characterized by high Al contents relative to K, Na, and Ca, are assumed to be derived from the melting of supra-crustal metasedimentary rocks [48]. For Wilson [49] the peraluminous granites contain crustal or sedimentary material in their magma of origin. This corroborates with the results of the Al2O3/CaO+Na2O+K2O versus SiO2 diagram [50], to differentiate between S-type and I-type granites. The SBO pegmatites plot within the S-type granite field (**Figure 14**). This type of granitoid implies that the parent magma from which the pegmatites were formed contained a large amount of sedimentary or crustal material. This suggests that the SBO pegmatites are derived from the partial melting of the Paleozoic metasedimentary rocks.

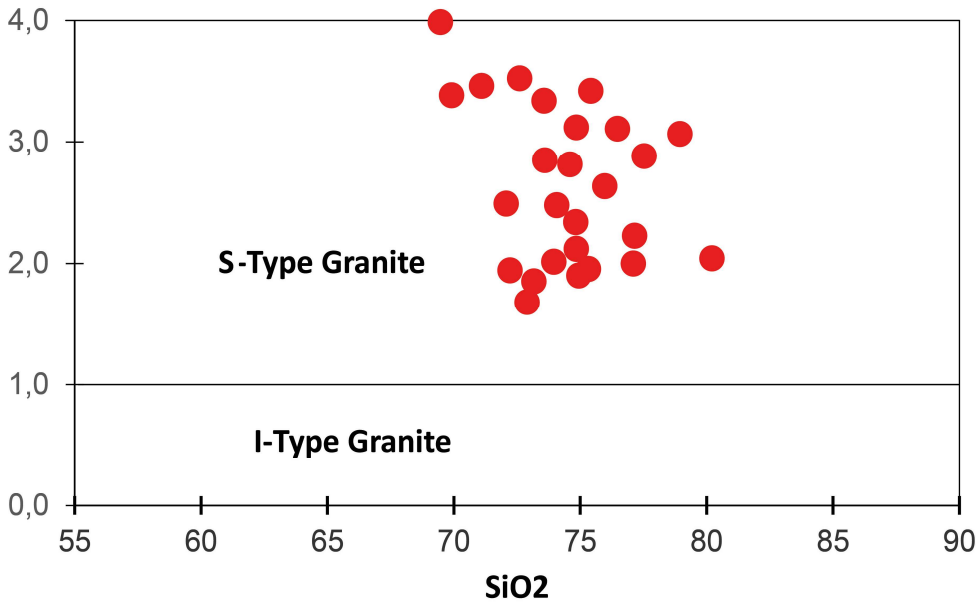

Figure 14. Classification diagrams. Al_2O_3/Cao+Na_2O+K_2O versus SiO_2 after White et al. [46].

Preprints (www.preprints.org) | NOT PEER-REVIEWED | Posted: 25 December 2023 doi:10.20944/preprints202312.1793.v1

5.1.2. Minor and Trace elements

As far as the minor and trace elements Rb, Sr, Ba have been plotted in the ternary diagram Rb-Sr-Ba proposed by El Bouseily et al. [51] , revealing that the SBO pegmatites occupy the field of strongly differentiated granites (**Figure 15**). Some samples also show a relative enrichment in Sr compared to their Ba content. It is worth noting that, according to El Bouseily et al. [51] , Rb, Sr, Ba are, monitors of the degree of magmatic differentiation.

In the geodynamic diagram Rb vs Nb + Y proposed by Pearce et al. [52] pegmatites are plotted in syn-collisional granite, with an exception for volcanic-arc granites (VAG) and within-plate granites (WPG) (**Figure 16a**). This is compatible with the results given by the Nb vs. Y diagram, after Pearce et al. [52]and Pearce [54] **(Figure 16b)** with some exception for within-plate granites (WPG), and the diagram Rb versus Yb + Ta, in which all samples fall in syn-collisional granite with a few exception for volcanic-arc granites (VAG) (**Figure 16c**), and Ta versus Yb, after Pearce et al. [52]. and Rb versus Y/Nb diagram by Pearce et al., [52] where all samples fall within syn-collisional granite affinity **(Figure 16d)**.

In the diagram after Batchelor et al., [53] (R1 =4Si-11(Na+K)-2(Fe+Ti) versus R2 = 6Ca+2Mg+Al), the SBO pegmatites fall in syncollisional to post-orogenic for the granite pegmatite field (**Figure 17**).

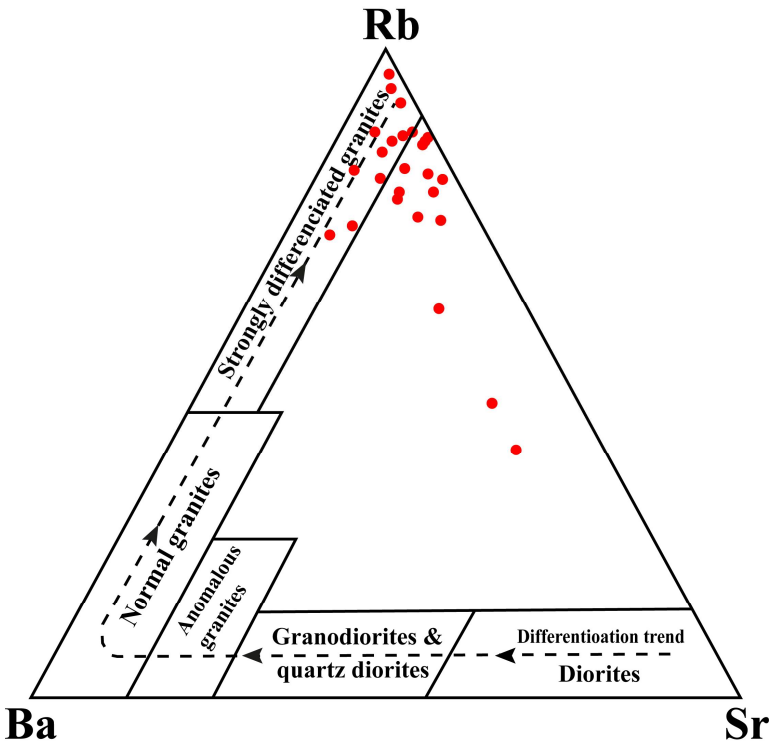

Figure 16. SBO pegmatite plotted in the Rb-Ba-Sr ternary diagram, after El Bouseilyet al., [51].

Preprints (www.preprints.org) | NOT PEER-REVIEWED | Posted: 25 December 2023 doi:10.20944/preprints202312.1793.v1

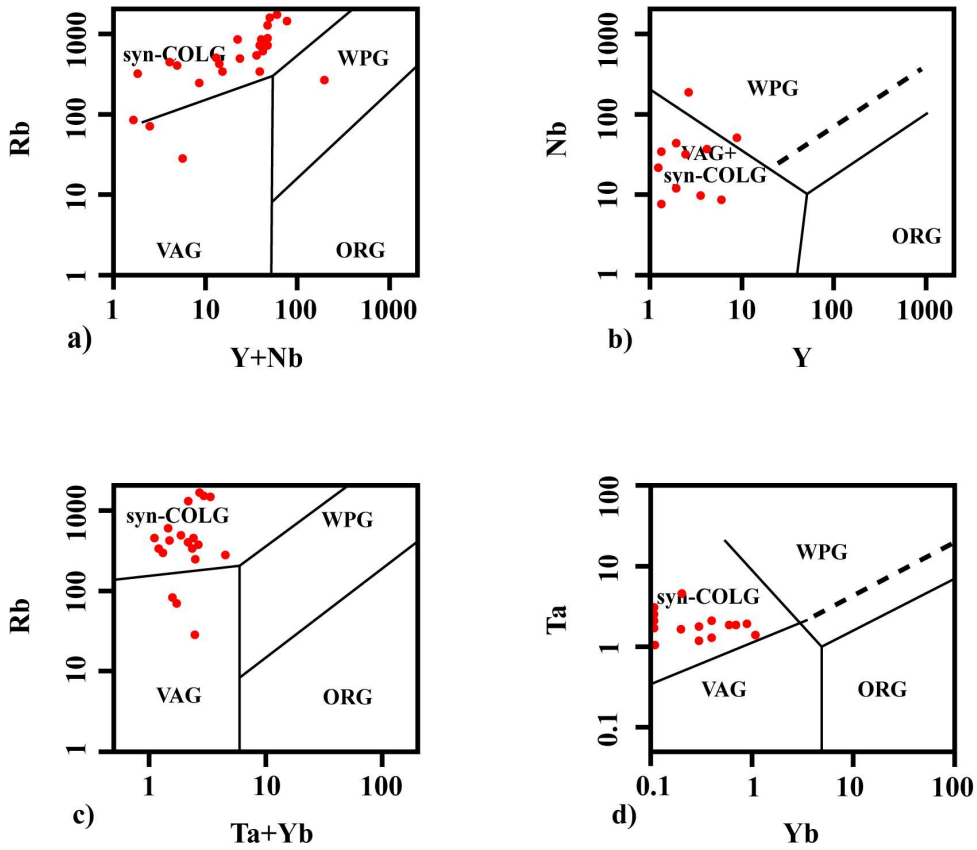

Figure 17. Tectonic discrimination diagrams for SBO pegmatites compositions. (a) Rb vs. Y+ Nb diagram, (b) Nb vs. Y diagram, after Pearce et al. [52]and Pearce [54], (c) Rb versus Yb + Ta, and (d) Ta versus Yb, after Pearce et al. [52]. Tectonic fields are ocean-ridge granites (ORG); syn-collisional granites (syn-COLG); volcanic-arc granites (VAG) and within-plate granites (WPG). The SBO pegmatites show syn-collisional granite affinity.

The trace element data that are related to SBO pegmatites samples were normalized to the upper crust [55]. The multi-element diagram (**Figure 18a**) shows strong to moderate positive anomalies in Rb, U, Sr, Sm, Tm. They indicate a negative anomaly in Nb, Ce, Nd, Zr, Ti. Negative Nb anomalies are characteristic of continental crust, while negative Nb and Zr anomalies indicate a calc-alkaline affinity.

Preprints (www.preprints.org) | NOT PEER-REVIEWED | Posted: 25 December 2023 doi:10.20944/preprints202312.1793.v1

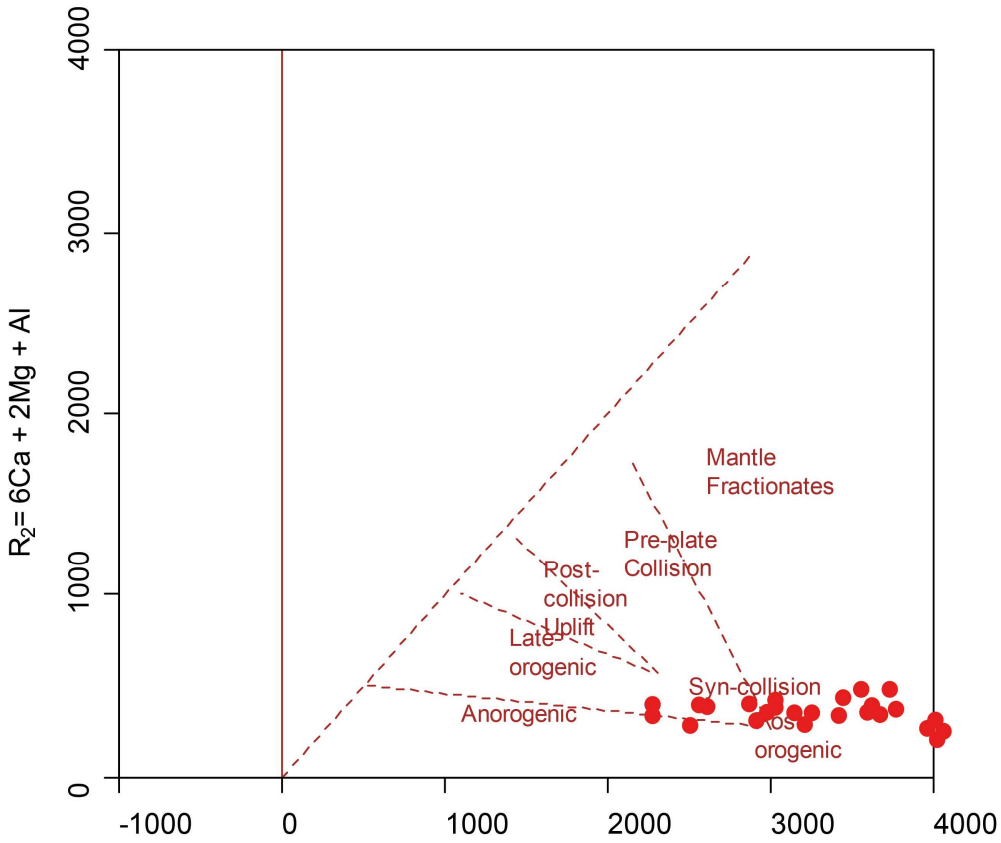

Figure 18. Discrimination geodynamic diagram [52], [53]R1= 4Si-11 (Na+K)-2(Fe+Ti) versus R2= 6Ca+2Mg+Al. The SBO pegmatites show syn-collisional and post-orogenic affinity.

Negative Ce anomalies are characteristic of certain orogenic rocks, which Hole at al., [56] and White et al., [57] attribute to an imprint of subducted sediments. However, the quantitative aspect seems to restrict this hypothesis. Ben Othman et al., [58], suggest that the relative Ce deficiency in some orogenic rocks may reflect the specific behavior of this element with respect to other REE during the fluid-rock interactions that take place at subduction zones.

Negative Nb-Ta anomalies the relative deficit of Nb and Ta compared to light REE is a typical feature of rocks associated with subduction zones [59], [60]. Some authors attribute this Nb and Ta deficit to selective trapping of these elements by stable titanium mineral phases in the hydrated, high-pressure, high-temperature conditions prevailing at subduction zones [59], [61], [62].

Zr-Hf anomalies contrary to a widely held view in the literature, Zr and Hf elements do not show a systematic deficit in relation to REE in orogenic rocks [59], [57]. In this type of representation, positive Zr and Hf anomalies are expressed by ordinate values greater than 1, negative anomalies by values less than 1. Thus, orogenic rocks do indeed show both positive and negative Zr and Hf anomalies.

The spider diagram of the SBO pegmatites shows a good correlation with the patterns for the collision granites calc-alkaline type [52]. There are some distinctive characteristics, the high contents of Rb in many of the patterns from the syn-collision granites and the very low contents of Ce and Zr.

The REEsof the SBO pegmatites were normalized to the chondrites of McDonough et al., [63]. The similarity of the rare-earth pattern of the multielement (**Figure 18b**) suggest a common source of their magmas. The patterns show a relatively weak enrichment in LREE compared to HREE. They sometimes show a negative Eu anomaly and sometimes a positive anomaly. The pattern of rare earth spectra (REE) agrees with the petrographic observations e.g., presence of plagioclases is expressed on the REE spectra with a positive Eu anomaly. The samples show an average enrichment in light rare earth elements (LREE). The patterns show a good correlation between the REE distribution and the Eu anomaly. Thus, samples with a positive europium anomaly have a slightly higher REE concentration.

Preprints (www.preprints.org) | NOT PEER-REVIEWED | Posted: 25 December 2023 doi:10.20944/preprints202312.1793.v1

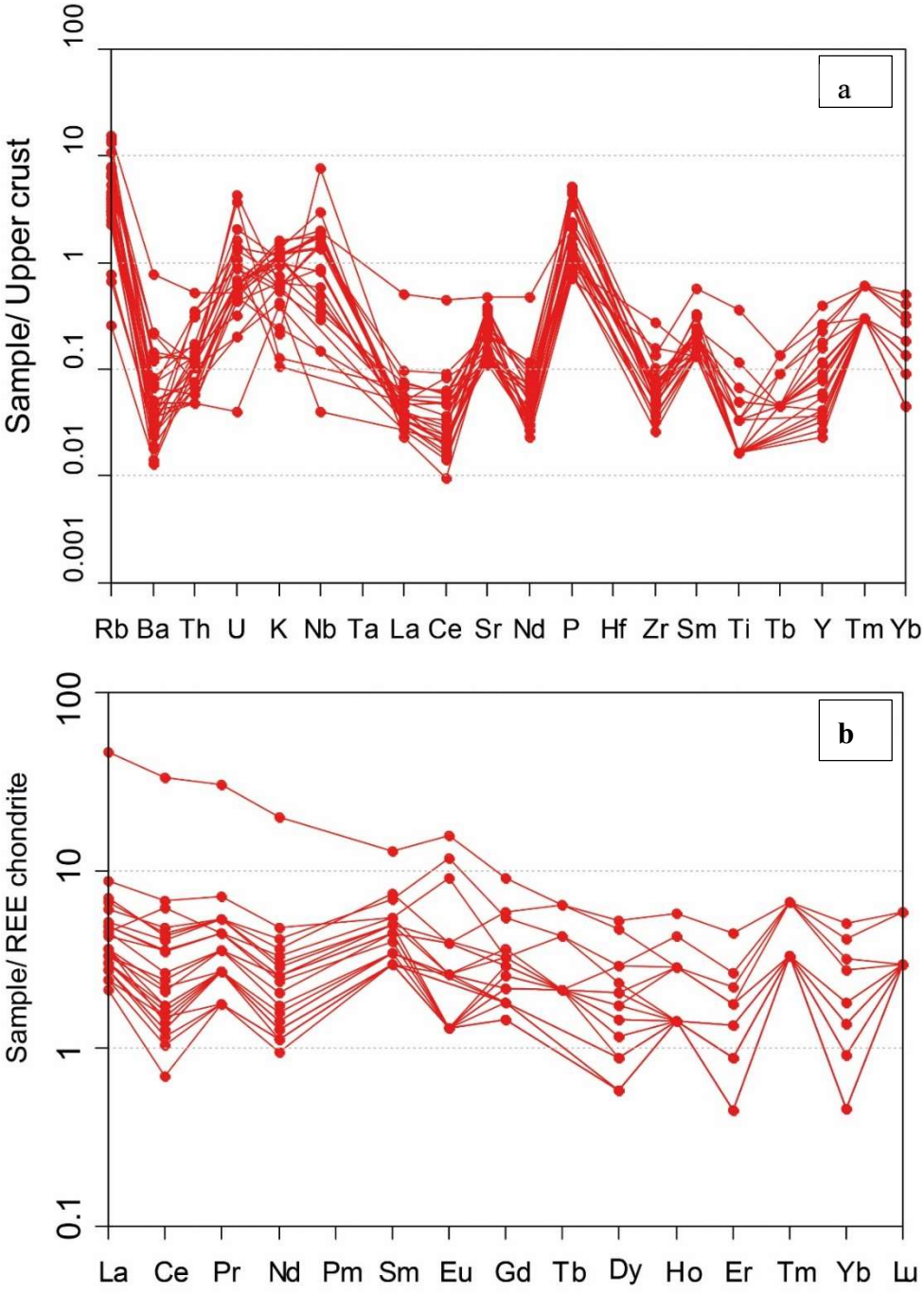

9

Figure 18. Multielements spider and REEs normalization diagrams explaining magma source and differentiation (**a**) Upper Continental Crust spider plot normalized and (**b**) REE chondrite spider plot after McDonough et al., [63].

5.2. Hydrothermal alteration and metasomatism

In addition to providing information on the physicochemical conditions of the system, the distribution of trace elements and EARs in the SBO pegmatites revealed important information on the rock/fluid interaction (**Figure 19**). Due to the dissolution or replacement of primary main and accessory minerals and the consequent development of new mineral phases, virtually all trace elements were mobilized during hydrothermal alteration and the petrographic study indeed confirms these changes. Moreover, the different types of hydrothermal alteration that affected these pegmatites can also be characterized using several geochemical diagrams proposed in the literature. The diagram of Stemprok [64] using the normative composition Qz-Ab-Or allows to determine the sodic, potassic,

 doi:10.20944/preprints202312.1793.v1

silicic and greisen alteration. The pegmatite samples are distributed in fields indicating silicification and greisinization, respectively (**Figure 19**).

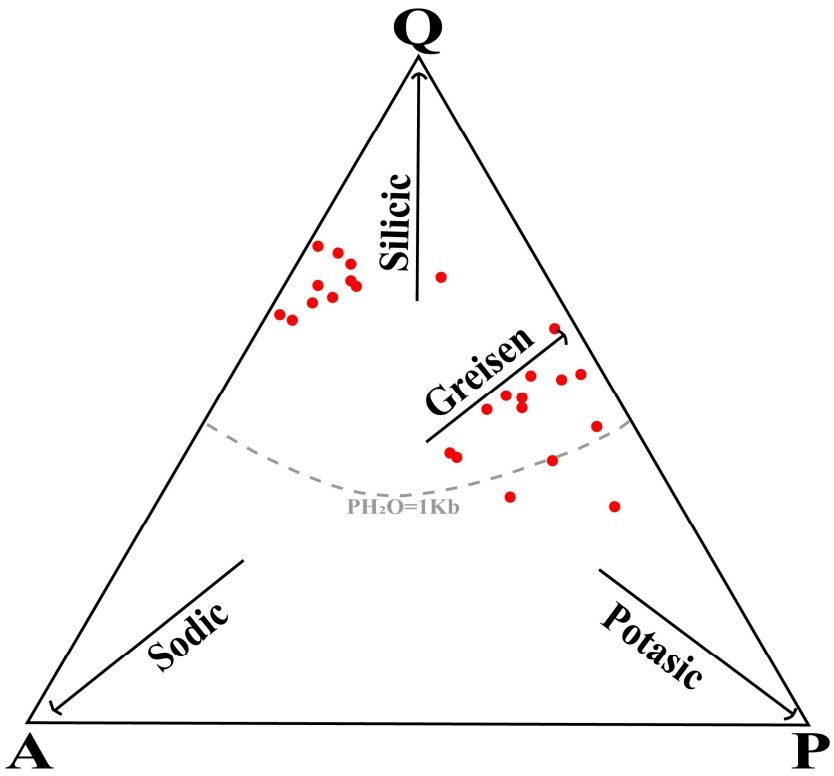

Figure 19. Ternary diagrams showing Normative Qz-Ab-Or ternary diagram [64].

These results are confirmed by microscopic observations where the occurrence of quartz and the quartz-muscovite association that comes from the transformation of minerals of the primary paragenesis is evident. Nevertheless, other samples have significant contents of Na_2O and are shifted towards albite. Albitization occurs during sodium metasomatism when Na^+ substitutes for K^+ and Ca^{2+} in pre-existing feldspars, while silicification leads to an increase in SiO_2 at the expense of the other major oxides and is followed by an increase in a few trace elements, including Zr, Ba and Rb. The K_2O vs. Na_2O diagram of Cuney et al., [42] show that these pegmatites are affected by mainly clay sodic and potassic alteration (**Figure 20**).

Preprints (www.preprints.org) | NOT PEER-REVIEWED | Posted: 25 December 2023 doi:10.20944/preprints202312.1793.v1

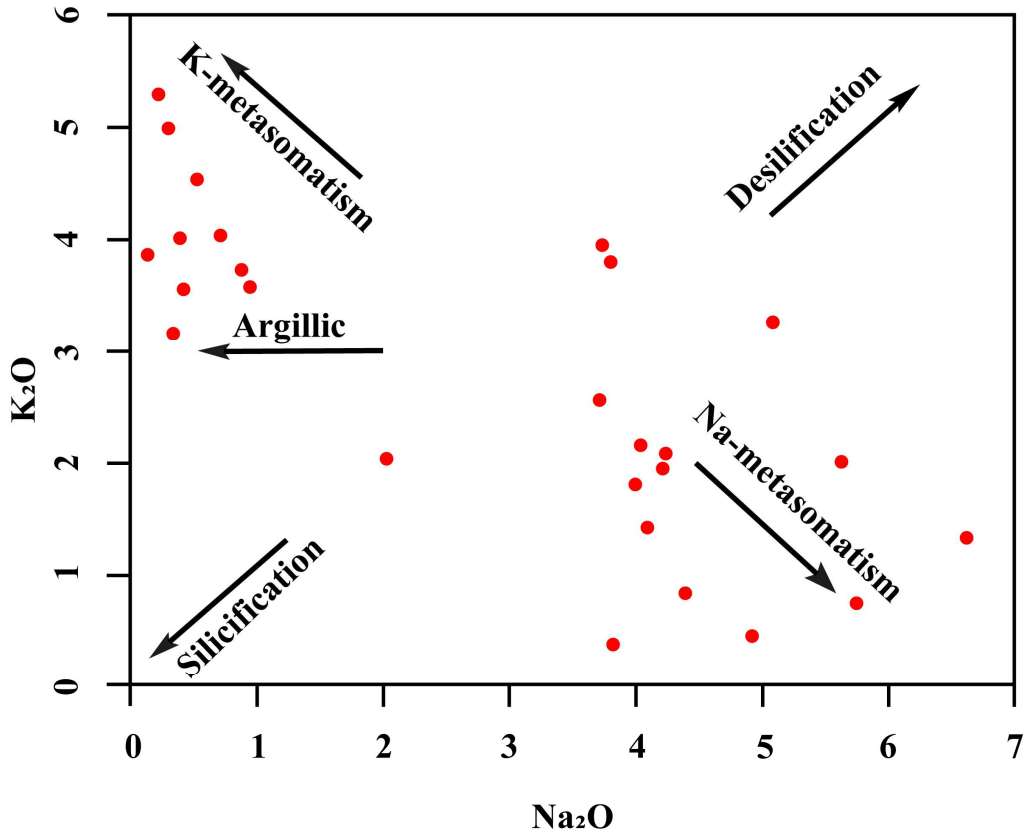

Figure 20. Bivariate K2O–Na2O variation diagram [42].

Moreover, the argillic alteration is the most dominant and the most marked (**Figure 21**) according to the ternary diagrams Al_2O_3- (Na2O + CaO)- K_2O and Al_2O_3 - (Na_2O+K_2O) - (Fe_2O_3t+MnO+MgO) and ofMeyer and at., [66].

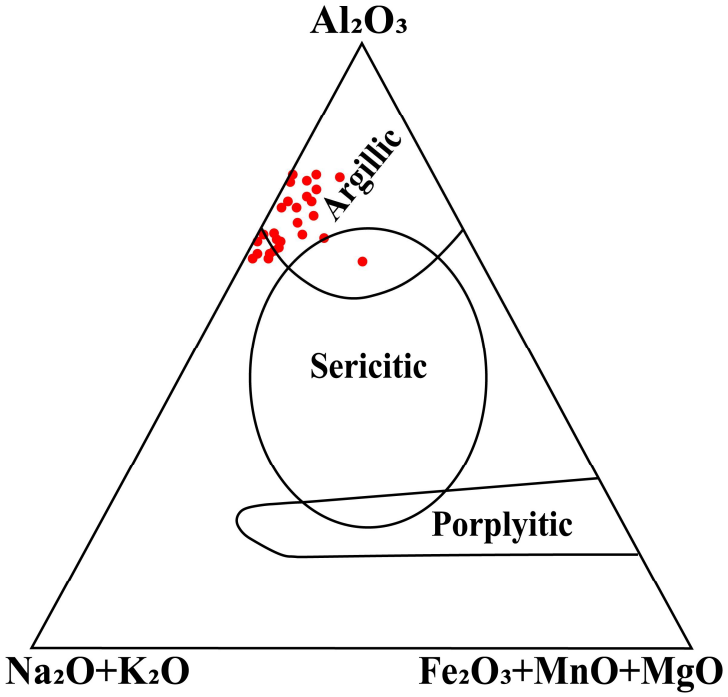

Figure 21. Al_2O_3 – (Na_2O+K_2O) – (Fe2O3 t +MnO+MgO) ternary diagram showing alteration type [66].

 doi:10.20944/preprints202312.1793.v1

It is obvious that the action of hydrothermal fluids was intense and generalized to all the pegmatitic bodies as suggested by Fransolet [12] and confirmed by Fontan [67], who explained that the transformation of triphylite into ferrisicklerite could only be complete under the action of hypogenous hydrothermal fluids, and that ferrisicklerite and hterosite can only be formed by hydrothermal alteration.

5.3. Classification

The current schemes used to classify pegmatites are as varied as numerous. Several authors have proposed various classification schemes based on the typical and auxiliary minerals of the pegmatite, on the P-T conditions of its emplacement and, more recently, on its geochemistry [68], [69], [70], [71]. However, the classification of pegmatites by Ginsburg et al., [72], which groups them according to their depth of emplacement, association with metamorphism, and relationship to granitic plutons, has had a significant influence on contemporary methods of pegmatite classification. The currently used taxonomy of pegmatites has the support of researchers and is known as the revision of Černy [73]. Its classification is based on a combination of minor element concentration and metamorphic grade at depth of emplacement. Four main classes or types are identified: 1) Abysal (AB) is the high-grade temperature (700-800°C), high to low pressure (4-9 kbar) and depth ≥11 km); 2) Muscovite (MSC) is a lower temperature (580-650°C) high pressure (5-8 kbar) and depth (7-11 km); 3) Rare-Element (REL) is a low temperature (500-650°C) and pressure (2-4 kbar) and depth (3. 5-7 km); 4) Miarolitic (MI) is a shallow level 500-650 °C at low temperature (≤500°C) and pressure (1-2 kbar) and depth (1.5-3.5 km).

The study of SBO pegmatites shows that these rocks are essentially composed of large crystals of feldspar, quartz, and muscovite with sometimes tourmaline. They are hosted exclusively in schists and no outcrops of granite have been observed in this area. Moreover, the geochemical results of these rocks indicate that they do not present any significant enrichment, that they are poor in REE but are on the other hand quite famous for their content in ceramic minerals [20]. These characteristics allow to classify the SBO pegmatites in the class of muscovite pegmatites. The latter are according to Černy [73] rarely mineralized but can produce feldspars and muscovite. They are considered to be of metamorphic origin, characterized by high-pressure metamorphism, hosted in almandine and kyanite schists and may contain Th,U,Nb,Ta,Zr,Ti [73]. Direct anatexis is thought to be the origin of first-drop rare-element mineralised pegmatites [68] and could also explain the diversity of magmatic fractionation observed in each type of pegmatite [74]. The crustal anatexis model was suggested in the 1970s [75, 76, 77, 78], to justify the extent of pegmatite fields compared with that of granitic plutons [79]. It has also been used to justify:(i) the absence of granite related to LCT pegmatite fields, (ii) the diachronism between granites and pegmatites [80], and (iii) the lack of continuity of magmatic fractionation between granites and the most differentiated pegmatites [81, 82]. Furthermore, the diversity of mineralisation and geochemical signatures associated with the pegmatite complex is mainly linked to the P-T conditions of regional metamorphism rather than to the fractional crystallisation of granitic bodies during their crystallization [83].

5.4. Origin of SBO pegmatites

The most widely accepted model for the genesis of pegmatites in the 1970s and 1980s was fractional crystallization of a granitic fluid. However, it is becoming accepted that they can be formed by metamorphic rock anatexis [74]. Considering the different models proposed that simplify the formation and mineralization of pegmatites, two final models have been proposed for pegmatite formation, continuous crystallization, and fractional dissolution [75].

According to Shmakin et al., [76], Gorlov [77], and Sokolov et al., [78], pegmatites of the muscovite class are produced directly by partial melting or by a very limited level of differentiation of anchiautochthonic palingenitic granites [72], [79], [80], [81]. This leads us to suggest that SBO pegmatite resulted from the partial melting of argillaceous metasedimentary rock of Sarhlef shist during variscan subduction and shortening. This corroborates with the geodynamic models proposed to explain the evolution of the Meseta from Upper Devonian to Lower Permian. The Eastward subduction of

the Rheic Ocean leading to the formation of fore- and back-arc basins in the Mesetian block between 420 and 330 Ma model [92, 93, 94] corroborates also with the Evolution model of the Meseta during the Carboniferous, proposed by Essaifi et al., [95] involving west-ward subduction followed by a slab breakoff leading to upwelling of hot asthenospheric currents eroding the litho-sphere.

6. Conclusions and final remarks

The Sidi Bou Othmane Variscan pegmatite crop out as dykes mainly oriented N30° (N-S to NNE-SSW) with sub-vertical dip. The field investigations show that E-W dykes are secant on NS pegmatite dykes. Their thickness varies from a few centimeters to a few meters (30 cm to 8 m) and has an extension of a few meters to a few hundred meters (1m to 500m). These dykes underwent a deformation presented on the ground by boudinage and strike-slip faults shifted their architectures.

SBO pegmatites are observed within the metamorphic rocks of the Sarlef series. They are clearly delimited bodies, which are mainly zoned and rarely homogeneous. They are never isolated but in a group of several dikes which are organized in fields of groups (clusters). SBO pegmatites show clearly tectonic control and are syn- or tardiorogenic and have calco-alkalic affinity and are S type granite. Using the mineralogy and the geochemistry, these pegmatites fall in very strongly differentiated granite field. Their features geochemical are compatible with their petrographical and mineralogical characteristics. They are mainly constituted by quartz, albite, muscovite, tourmaline, with minor microcline, illite, with accessory garnet, apatite, and zircon. These characteristics allow to classify the SBO pegmatites in the class of muscovite pegmatites. The classification of the SBO pegmatites within this class, indicate that they do not present any significant enrichment in REE. They are probably the products of partial melting of pelitic metasedimentary rock of Sarhlef during variscan shortening between 330 and 280-275 Ma.

Finally, in the frame of the shift to green technologies it is worth noting that, apart from some accessory minerals of interest that are hosted in pegmatite-type deposits, some main occurring minerals such as feldspars and quartz are increasingly required for the production and storage of renewable (green) energy to supply the green and sustainable societies of the future [82], [83]. For instance, feldspars have been recently assessed by the European Commission as critical raw materials (CRMs) (https://single-market-economy.ec.europa.eu/publications/study-critical-raw-materials-eu-2023-final-report_en).

Therefore, in the frame of the current global trend, the SBO pegmatite may constitute an important georesource to be considered at a greater detail.

Author Contributions: For research articles with several authors, a short paragraph specifying their individual contributions must be provided. The following statements should be used "Conceptualization, A.W.; methodology, A.W.; software, N.E.A. Y.M. and M.C.; validation, A.W., Y.M. and M.C.; formal analysis, A.W.; investigation, A.W., M.C. and W.A.S.; resources, A.W.; data curation, A.W., M.C., and W.A.S.; writing—original draft preparation, A.W., Y.M., R.P., D.G. and A.M.C.; writing—review and editing, A.W., R.P., D.G. and A.M.C.; visualization, A.W.; supervision, A.W.; project administration, A.W.; funding acquisition, Y.D. All authors have read and agreed to the published version of the manuscript." Please turn to the CRediT taxonomy for the term explanation. Authorship must be limited to those who have contributed substantially to the work reported.

Funding: "This research received no external funding".

Acknowledgments: We acknowledge Reminex, Managem Group for ICP-MS analysis.

Conflicts of Interest: The authors declare no conflict of interest.

References

1. London, D. Pegmatites. *Can. Mineral. Special Publication* **2008**, *10*, 1-347.
2. London, D. The origin of primary textures in granitic pegmatites. *Can. Mineral.* **2009**, *47*, 697-724 https://doi.org/10.3749/canmin.47.4.697.
3. London, D. Crystal-filled cavities in granitic pegmatites: Bursting the bubble. *Rocks Miner.* **2013**, *88(6)*, 527-538.
4. Steiner, B.M. Tools, and workflows for grassroots Li-Cs-Ta (LCT) pegmatite exploration. *Minerals* **2019**, *9(8)*, 24-26.

5. Linnen, R.L.; Van Lichtervelde, M.; Černý, P. Granitic Pegmatites as Sources of Strategic Metals. *Elements* **2012,** *8(4)*, 275-280 https://doi.org/10.2113/gselements.8.4.275.
6. London, D. A petrologic assessment of internal zonation in granitic pegmatites. *Lithos* **2014**, *184*, 74-104.
7. London, D. Ore-forming processes within granitic pegmatites. *Ore Geol. Rev.* **2018**, *101*, 349-383.
8. Bouladon, J.; Jouravsky, G.; & Morin, P. Etude préliminaire des pegmatites a muscovite et béryl du Sud de la Plaine de Tazenakht. *Notes Mem. Serv. Geol. Maroc.* **1950**, *3(76)*, 207-235.
9. Bouladon, J.; Jouravsky, G.; & Vergerto, R. Note sur les recherches de béryl et de mica dans le Sud de la plaine de Tazenakht. *Rapport, Serv Géol Maroc, Div.Serv. Etudes Gîtes* **1952**, *6*, 297-
10. Permingeat, F. Sur les niobo-tantalates de l'Anti-Atlas, Maroc: tapiolite et columbite. *Bull. Soc. Fr. Mineral. Cristallogr.* **1955**, *78*, 123-156.
11. Cech, F. ; Johan, Z. ; & Povondra, P. La barbosalite de la pegmahte d'Angarf-Sud,Plaine de Tazenakht, Anti-Atlas, Maroc. *Notes Serv. Geol. Maroc* **1972**, *32(241)*, 121-128.
12. Fransolet, A.M. Les phosphates lithiques des pegmatites de la Plaine des Zenaga (Anti-Atlas, Maroc). *Notes Serv Geol. Maroc* **1974**, *35(255)*, 137-143.
13. Fransolet, A.M. ; Antenucci, D. ; Speetjens, J.M. ; & Tarte, P. An X-ray determinative method for the divalent cation ratio in the triphylite-lithiophilite series. *Mineral. Mag.* **1984**, *48(348)*, 373-381.
14. Fransolet, A.M.; Abraham, K.; & Speetjens, J.M. Evolution génétique et signification des associations de phosphates de la pegmatite d'Angarf-Sud, plaine de Tazenakht, Anti-Atlas, Maroc. *Bulletin de Minéralogie* **1985**, *108(3)*, 551-574.
15. Kampf, A.; & Mills, S. ANGARFITE, NaFe3+5(PO4)4(OH)4•4H2O, a new mineral species from the Angarf-sud pegmatite, Morocco: description and crystal structure. *Can. Mineral.* **2012**, *50*, 781-791.
16. Morsly, Y.; Zerhouni, Y.; Maimouni, S.; Alikouss, S.; & Kadir, H. Pegmatite mapping using spectroradiometry and ASTER data (Zenaga, Central Anti-Atlas, Morocco). *J. African Earth Sci.* **2021**, *177*, 104-173. https://doi.org/10.1016/j.jafrearsci.2021.104153
17. Morsli, Y. ; Zerhouni, Y.; Wafik, A.; Elouazzani, A.; Alikouss, S.; Saidi, A.; & Baroudi, Z. Eburneen pegmatites of the Zenaga inlier (Anti-Atlas, Morocco): Petrography, geochemistry, and classification. *J. African Earth Sci.* **2022**, *186*, 104-438. https://doi.org/10.1016/j.jafrearsci.2021.104438
18. Permingeat, F. Presence du lithium dans les pegmatites de Sidi Bou Othmane (Jebilet). *Mines et Geologie* **1959**, *8*, 46-47.
19. Huevelin, P.; & Mazeas, J. Presence de cassiterite et de beryl dans les pegmatites hercyniennes de la region de Sidi Bou Othmane (Jebilet centrales, Maroc). *C. R. Somm. Soc. Geol. Fr.* **1964**, *10*, 419–420.
20. Agard, J.; & Morin, P. Beryllium et mica. *Notes Du Service Geologique Du Maroc* **1980**, *276*, 257–269.
21. Fontan, F.; Huvelin, P.; & Permingeat, F. Rockbridgeite, phosphosiderite et mitridatite des pegmatites de Sidi Bou Othmane (Jebilet). *Notes Serv. Geol. Maroc* **1972**, *32*, 150-151.
22. Fontan, F. Phosphates mineurs des pegmatites de Sidi Bou Othmane. *Notes Serv. Geol. Maroc.* **1975**, *40*, 249-252.
23. Fontan, F.; Huvelin, P.; Orliac, M.; & Permingeat, F. La ferrisicklerite des pegmatites de Sidi Bou Othmane (Jebilet, Maroc) et le groupe des mineraux astructure de triphylite. *Bull. Soc. Fr. Mineral. Cristallogr*. **1976**, *99*, 274–286.
24. Essafi, A.; Lacinska, A. M.; Corsini, M.; Goodenough, K. M.; Arbaoui, A. E.; & Zayane, R. Mobilisation of rare earth elements in shear zones: Insights from the Tabouchent granodioritic pluton (Jebilet massif, Variscan Belt, Morocco). *Ore Geol. Rev.* **2021**, *133*, 103996. https://doi.org/10.1016/j.oregeorev. 2021.103996
25. Bouloton, J.; & Gasquet, D. Melting and undercooled crystallisation of felsic xenoliths from minor intrusions (Jebilet massif, Morocco). *Lithos* **1995**, *35*(3-4), 201-219.
26. Delchini, S. Etude tectono-thermique d'un segment orogénique varisque à histoire géologique complexe: analyse structurale, géochronologique et thermique du massif des Jebilet, de l'extension à la compression. PhD Thesis, Université d'Orléans, 27 Avril 2018.
27. Zouicha, A.; Saber, H.; Attari, A. E.; Zouheir, T.; & Ronchi, A. Late Hercynian tectonic evolution of the Jebilet Massif (Western Meseta, Morocco) based on tectono-sedimentary analyses of related Permian continental deposits. *J. Iber. Geol.* **2022**, *48*(4), 377-403.
28. Huvelin, P. Etude géologique et gîtologique du Massif hercynien des Jebilet (Maroc occidental). *Notes Mém. Serv. Géol. Maroc*. **1977**, *232 bis*, 1–307.
29. Lazreq, N.; Königshof, P.; Essaifi, A.; Bouari, A.; & Outigua, A. A Devonian age for the Sarhlef Formation (Jebilet Massif, Morocco) – evidence from new biostratigraphic data based on metamorphosed conodonts. *Palaeogeogr. Palaeoclimatol. Palaeoecol.* **2021**, *572*, 110395. https://doi.org/10.1016/j.palaeo.2021.110395
30. Bordonaro, M. Tectonique et pétrographie du district à pyrrhotine de Kettara. Thèse de 3ème cycle, Univ. Louis-Pasteur, Strasbourg, 1983.
31. Lagarde, J.L.; Ait Omar, S.; & Roddaz, B. Structural characteristics of granitic plutons emplaced during weak regional deformation: examples from late Carboniferous plutons, Morocco. *J. Struct. Geol.* **1990**, *12*(7), 805–821. https://doi.org/10.1016/0191-8141(90)90056-5

32. Pique, A.; & Michard, A. Moroccan Hercynides: a synopsis. The Paleozoic sedimentary and tectonic evolution at the northern margin of West Africa. *Am. J. Sci.* **1989**, 289(3), 286–330. https://doi.org/10.2475/ajs.289.3.286
33. El Hassani, I.E.E.A. Petrogenèse des granitoïdes peralumineux des Jebilet centrales (Maroc) approche par l'étude des enclaves. *Bulletin de l'Institut Scientifique* **1996**, *20*, 1–23.
34. Mrini, Z.; Rafi, A. ; Duthou, J. ; & Vidal, P. Chronologie Rb-Sr des granitoı¨des hercyniens du Maroc : conséquences. *Bulletin De La Societe Geologique De France* **1992**, *163*, 281–291.
35. Gaillet, J.; & Bordonaro, M. La tectogenèse hercynienne dans le massif dinantien des Jebilet centrales (Maroc). *Sciences Géologiques Bulletin* **1981**, *34*(2), 117–122. https://doi.org/10.3406/sgeol.1981.1595
36. Bouloton, J.; & Le Corre, C. Le problème de la tectonique tangentielle dans les Jebilet (Maroc hercynien): données et hypothèses. *Hercynica* **1985**, *1*, 121–129.
37. Lagarde, J.L.; Ait Ayad, N.; Ait Omar, S.; Chemsseddoha, A.; & Saquaque, A. Les plutons granitiques tardi carbonifères marqueurs de la déformation crustale. L'exemple des granitoïdes de la méseta marocaine. *Comptes Rendus de l'Academie Des Sciences* **1989**, *309*, 291–296.
38. El Mostadi, A. Etudes géologique, pétrographique et gitologique des Skarns minéralisés en scheelite et cassitérite du secteur de Sidi Bou Othmane (Jebilet Centrales, MAROC) guides de recherches. Thèse 3 ème cycle, Université Cadi Ayyad Faculté des Sciences Marrakech, 1992.
39. Beauchamp, J.; & Izart, A. Early Carboniferous basins of the Atlas-Meseta domain (Morocco): sedimentary model and geodynamic evolution. *Geol.* **1987**, *15*(9), 797–800. https://doi.org/10.1130/0091-7613(1987)15<797:ECBOTA>2.0.CO;2
40. Hanson, G. The application of trace elements to the petrogenesis of igneous rocks of granitic composition. *Earth Planet Sci. Lett.* **1978**, *38*, 26–43.
41. Herrmann, A.G. Yttrium, and lanthanides. In *Handbook of Geochemistry;* Wedepohl, K.H., Eds; Publisher: Springer-Verlag, Berlin, Germany, 1970; Volume 2(5), pp. 39–57.
42. Cuney, M.; Friederich, M. Physicochemical and crystal-chemical controls on accessory mineral paragenesis in granitoids: implications for uranium metallogenesis. *Bull. Minéral,* **1987**, *110,* 235–47. https://doi.org/10.3406/bulmi.1987.7983
43. Chatelineau, M. U-Th-RRE mobility during albitization and quartz dissolution in granitoids: Evidence from southeast French Massif Central. *Bull. Mineral.*, 1987, *110*, 249–259. https://doi.org/10.3406/bulmi.1987.7984
44. Middlemost, E.A.; Magmas, K.; & Rocks, M. An introduction to igneous petrology. *Magma and magmatic Rocks.* Longman Group Ltd., London, United Kingdom, 1985; pp. 1-266.
45. Maniar, P.D.; & Piccoli, P.M. Tectonic discrimination of granitoids. *Geol. Soc. Am. Bull.*, **1989**, *101*, 635–643.
46. White, R.J.A.; and Chappell, W.B. Ultrametamorphism and Granitoid Genesis. *Tectonophysics* **1977**, *43*, 7-22. https://doi.org/10.1016/0040-1951(77)90003-8
47. Irvine, T.N.; and Baragar, W.R.A. A Guide to the Chemical Classification of the Common Volcanic Rocks. *Can. J. Earth Sci.* **1971**, 8, 523-548.
48. Barbarin, B. Genesis of the two main types of peraluminous granitoids. *Geol.* **1985**, *24*, 295–298.
49. Wilson, M. *Igneous Petrogenesis Global Tectonic Approach*, 1st ed.; Harpar Collins Academy, London, United Kingdom, 1989; pp. 227–241.
50. Chappell, B.; & White, A.J. Two contrasting granite types. *Pac. Geol.* **1974**, *8*, 173–174.
51. El Bousely, A. ; & El Sokkary, A. The relation between Rb, Ba, and Sr in granitic rocks. *Chem. Geol.*, **1975**, *16 (3)*, 207–219.
52. Pearce, J.; Harris, N.; & Tindle, A. Trace element discrimination diagrams for the tectonic interpretation of granitic rocks. *J. Petrol.* **1984**, *25, 956–983.*
53. Batchelor, R.; & Bowden, P. Petrogenetic interpretation of granitoid rock series using multicationic parameters. *Chem. Geol.* **1985**, *48 (1–4),* 43–55.
54. Pearce, J.A. A User's Guide to Basalt Discrimination Diagrams. In *Trace Element Geochemistry of Volcanic Rocks: Applications for Massive Sulphide Exploration;* Wyman, D.A., Ed.; Geological Association of Canada, 1996; Volume 12, pp. 79-113.
55. Taylor, S.R.; & McLennan, S. M. The geochemical the continental evolution crust. *Rev Mineral Geochem* **1995**, *33*(2), 241–265.
56. Hole, M.J.; Saunders, A. D.; Marriner, G. F.; & Tarney, J. Subduction of pelagic sediments: implications for the origin of Ce-anomalous basalts from the Mariana Islands. *J. Geol. Soc.* **1984**, *141*(3), 453–472. https://doi.org/10.1144/gsjgs.141.3.0453
57. White, W.M.; & Patchett J. Hf Nd Sr isotopes and incompatible element abundances in island arcs: implications for magma origins and crust-mantle evolution. *Earth Planet. Sci. Lett.* **1984**, *67*(2), 167–185. https://doi.org/10.1016/0012-821X(84)90112-2
58. Ben Othman, D.; White, W.; & Patchett, J. The geochemistry of marine sediments, island arc magma genesis, and crust-mantle recycling. *Earth Planet. Sei. Lett.* **1989**, *94*, 1–21.

59. Briqueu, L.; Bougault, H.; & Joron, J. L. Quantification of Nb, Ta, Ti and V anomalies in magmas associated with subduction zones: Petrogenetic implications. *Earth Planet. Sei. Lett.* **1984**, *68*(2), 297–308. https://doi.org/10.1016/0012-821X(84)90161-4
60. Wood, D.A. A variability veined sub-oceanic upper mantle-genetic significance for mid-ocean ridge basalts from geochemical evidence. *Geology* **1979**, *7*, 499–503.
61. Morris, J.D.; & Hart, S. R. Isotopic and incompatible element constraints on the genesis of island arc volcanics from Cold Bay and Amak Island, Aleutians, and implications for mantle structure: Reply to a Critical Comment by M. R. Perfit and R. W. Kay. *Geochim. Cosmochim. Acta* **1983**, *50*(3), 483–487. https://doi.org/10.1016/0016-7037(86)90202-4
62. Saunders, A.D.; Tarney, J.; & Weaver, S. D. Transverse geochemical variations across the Antarctic Peninsula: Implications for the genesis of calc-alkaline magmas. *Earth Planet. Sei. Lett.*, **1980**, *46*(3), 344–360. https://doi.org/10.1016/0012-821X(80)90050-3
63. Mc Donough, W.; & Sun, S. The composition of the Earth. *Chem. Geol.* **1995**, *120*, 223–253.
64. Stemprok, M. Mineralized granites and their origin: review of MAWAM contributions. *Episodes* **1979**, *12*, 49-53. https://doi.org/10.18814/epiiugs/1979/v2i3/005
65. Nasbitt, H.W.; Young, G.M. Formation and diagenesis of weathering profiles. *J. Geol.* **1989**, *97*, 129–147. https://doi.org/10.1086/629290
66. Meyer, C.; Hemely, J.J. *Wall rock alteration in geochemistry of Ore Deposits.* H L Barnes, ed.; Holt, Ranehart & Winston, New York, 1967; pp. 166-235.
67. Fontan, F. Phosphates mineurs des pegmatites de Sidi Bou Othmane. *Notes Serv. Geol. Maroc.* **1976**, *40*, 249-252.
68. Wise, M.A.; Müller, A.; & Simmons, W. B. (2022). A proposed new mineralogical classification system for granitic pegmatites. *Can. Mineral.* **2022**, *60*(2), 229-248.
69. Simmons, W. B. A look at pegmatite classifications. In Proceedings of Crystallization Processes in Granitic Pegmatites-International Meeting, Elba Island, Italy, 23rd-29th May 2005.
70. Cˇerný, P.; & Ercit, T. S. The classification of granitic pegmatites revisited. *Can. Mineral.* **2005**, *43*(6), 2005-2026.
71. Simmons, W. B. S.; & Webber, K. L. Pegmatite genesis: state of the art. *Eur. J. Mineral.* **2008**, *20*(4), 421-438.
72. Ginsburg, A.; Timofeyev, I.; & Feldman, L. *Principles of Geology of the Granitic Pegmatites*. Nedra eds.; Moscow, Russia, 1979; p. 296.
73. Černy, P. Rare-element granitic pegmatites. Part II: Regional to global environments and petrogenesis. *Geosci. Canada* **1991,** *18(2).* https://journals.lib.unb.ca/index.php/GC/article/view/3723
74. Roda-Robles, E.; Pesquera, A.; Velasco, F.; Fontan, F. The granitic pegmatites of the Fregeneda area (Salamanca, Spain): characteristics and petrogenesis. *Mineral. Mag.* **1999,** *63*, 535–558.
75. Norton, J.J. Composition of a pegmatite. *Am. Mineral.* **1970**, 55, 981—1002.
76. Zasedatel, A.M. Possible accumulation oflithium in host rocks of lithium pegmatite veins during old sedirnentation processes. Dokl, *Acad. Sci. USSR, Earth-Sci.Sect.* **1974**, 218, 196-198.
77. Zasedatel, A.M. Quantitative model of metamorphic generation of rare-metal pegmatite with lithium mineralization. Dokl, *Acad. Sci. USSR, Earth-Sci.Sect.* **1977**, 236, 219-221.
78. Stewart, D.B. Petrogenesis of lithium-rich pegmatites. *Am. Mineral.* **1978**, 63, 970—980.
79. Norton, J.J. & Redden, J.A. Relations of zoned pegmatites to other pegmatites,granite,and metamorphic rocks in the southernBlack Hills, SouthDakota. *Am. Mineral.* **1990**, 75, 631—655.
80. Melleton. J.; Gloaguen. E.; Frei, D.; Novák, M.; Breiter, K. How are the emplacement of rare-element pegmatites, regional metamorphism and magmatism interrelated in the Moldanubian domain of the Variscan Bohemian Massif, Czech Republic? *Can. Mineral.* **2012**, 50, 1751-1773.
81. Martins, T.; Lima, A.; Simmons, W.B.; Falster, A.; Noronha, F. Geochemical fractionation of Nb–Ta oxides in li-bearing pegmatites from the Barroso–Alvão pegmatite field, northern Portugal. *Can. Mineral.* **2011**, 49, 777-791.
82. Roda Robles, E.; Pesquera Perez, A.; Velasco Roldan, F.; Fontan, F. The granitic pegmatites of the Fregeneda area (Salamanca, Spain); characteristics and petrogenesis. *Mineral. Mag.* **1999**, 63(4), 535-558.
83. Nabelek, P. I.; Russ-Nabelek, C.; & Denison, J. R. The generation and crystallization conditions of the Proterozoic Harney Peak Leucogranite, Black Hills, South Dakota, USA: Petrologic and geochemical constraints. In *Contr. Mineral. and Petrol.,* 1st ed.; Publisher: Springer Nature, USA, 1992; Volume 110, pp. 173-191.
84. Simmons, W. B.; Foorf, E. E.; Falster, A. U.; & King, V. T. Evidence for an anatectic origin of granitic pegmatites, western Maine, USA. *Geol. Soc. Am. Bull.* **1995**, *27*, 411.
85. Shearer, C.; & Papike, J.; Jolliff, B.L. Petrogenetic links among granites and pegmatites in the Hamey Peak rare-element granite-pegmatite system, Black Hills, South Dakota. *Can. Mineral.* **1992**, *30*, 785-809.
86. Shmakin, B.M.; & Makagon, V.M. Physicochemical conditions of formation of the muscovite-bearing pegmatites. In Proceedings of Int. Geol. Congress, Moscow, Russia, 1972**,** 3(2), 591-599.

87. Gorlov, N.V. Structural principles of exploration for pegmatite deposits in northwestern White Sea region. In *Muscovite Pegmatites of the USSR*, Nauka eds.; Leningrad, Russia, 1975; pp. 146-153.
88. Sokolov, Y.M.; Kratz, K.O.; & Glebovitskyi, V.A. Regularities in the formation and distribution of the muscovite and muscovite – rare metal pegmatite formations in metamorphic belts. In *Muscovite Pegmatites of the USSR*, Nauka eds.; Leningrad, Russia, 1975; Volume, pp. 5-15.
89. Bushev, A.G. Linkage of muscovite pegmatites with granites. In *Muscovite Pegmatites of the USSR*, Nauka eds.; Leningrad, Russia, 1975; pp. 77-84.
90. Gordiyenko, V.V.; & & Leonova, V.A. *Mica-Bearing Pegmatites of Northern Karelia*. Nauka eds.; Leningrad, Russia, 1976, Nedra, Leningrad, USSR (in Russ.) p 367.
91. Shmakin, B.M. (1976): *Muscovite and Rare Metal*. Nauka, Novosibirsk, eds.; Leningrad, Russia, 1976, 376 p.
92. Michard, A.; Saddiqi, O.; Chalouan, A.; Frizon de Lamotte, D. *Continental Evolution: The Geology of Morocco*, 1st ed.; Publisher: Springer Berlin, Heidelberg, 2008; pp. 1-426.
93. Michard, A.; Soulaimani A.; Hoepffner, C.; Ouanaimi, H.; Baidder, L.; Rjimati, E.C.; Saddiqi, O. The South-Western Branch of the Variscan Belt: Evidence from Morocco. *Tectonophysics* **2010**, 492, 1-24.
94. Delchini, S.; Lahfid, A.; Lacroix, B.; Baudin, T.; Hoepffner, C.; Guerrot, C.; Lach, P.; Saddiqi, O.; Ramboz, C. The geological evolution of the Variscan Jebilet massif, Morocco, inferred from new structural and geochronological analyses. *Tectonics* **2018**, 37, 4470-4493.
95. Essaifi, A.; Samson, S.; & Goodenough, K. Geochemical and Sr–Nd isotopic constraints on the petrogenesis and geodynamic signifi-cance of the Jebilet magmatism (Variscan Belt, Morocco). *Geol. Mag.* **2013,** 151(4), 666–691.